ARTICLES
https://doi.org/10.1038/s41591-021-01645-7

nature medicine

Check for updates

Human pluripotent stem-cell-derived islets ameliorate diabetes in non-human primates

Yuanyuan Du[1,2,10], Zhen Liang[1,2,10], Shusen Wang[3,10], Dong Sun[1,10], Xiaofeng Wang[2,10], Soon Yi Liew[1,10], Shuaiyao Lu[4,10], Shuangshuang Wu[2], Yong Jiang[2], Yaqi Wang[5], Boya Zhang[3], Wenhai Yu[4], Zhi Lu[2], Yue Pu[6], Yun Zhang[3], Haiting Long[4], Shanshan Xiao[6], Rui Liang[3], Zhengyuan Zhang[1], Jingyang Guan[1], Jinlin Wang[1], Huixia Ren[7], Yanling Wei[2], Jiaxu Zhao[8], Shicheng Sun[1], Tengli Liu[3], Gaofan Meng[1,2], Le Wang[3], Jiabin Gu[2], Tao Wang[6], Yinan Liu[1], Cheng Li[5], Chao Tang[7], Zhongyang Shen[3]✉, Xiaozhong Peng[4,9]✉ and Hongkui Deng[1]✉

Human pluripotent stem-cell-derived islets (hPSC-islets) are a promising cell resource for diabetes treatment[1,2]. However, this therapeutic strategy has not been systematically assessed in large animal models physiologically similar to humans, such as non-human primates[3]. In this study, we generated islets from human chemically induced pluripotent stem cells (hCiPSC-islets) and show that a one-dose intraportal infusion of hCiPSC-islets into diabetic non-human primates effectively restored endogenous insulin secretion and improved glycemic control. Fasting and average pre-prandial blood glucose levels significantly decreased in all recipients, accompanied by meal or glucose-responsive C-peptide release and overall increase in body weight. Notably, in the four long-term follow-up macaques, average hemoglobin A1c dropped by over 2% compared with peak values, whereas the average exogenous insulin requirement reduced by 49% 15 weeks after transplantation. Collectively, our findings show the feasibility of hPSC-islets for diabetic treatment in a preclinical context, marking a substantial step forward in clinical translation of hPSC-islets.

Cell replacement therapy holds promise in the treatment of diseases such as type 1 diabetes mellitus (T1DM), which is mainly caused by the loss of islet β cells[4,5]. Human islet transplantation has been shown to reverse T1DM by effectively restoring endogenous insulin secretion in patients[6,7]. However, the number of patients who can benefit from islet transplantation is presently limited by the lack of a readily accessible source of human islets[8]. Moreover, despite continuous immunosuppression, the progressive loss of graft function and recurrence of immune attack to the β cells also hinder the widespread application of islet transplantation[7,9–12].

Human pluripotent stem cells serve as an abundant resource for the generation of functional cells, including the pancreatic islet β cell[5,13], thus providing a solution that circumvents the requirement for donor-derived tissues. However, many uncertainties remain in the translation of pluripotent stem-cell-based treatments for human transplantation and therapy that are difficult to investigate using rodent animal models[14]. Non-human primates possess a high degree of similarity in genetics, anatomy, metabolism and physiology to humans, making them a critical model for rigorous assessment of potential therapeutics and addressing translational issues before clinical trials in humans[3,14]. In this study, we investigated the feasibility, safety and efficacy of transplanting hPSC-islets for diabetes treatment in non-human primates.

Results

We first sought to establish a differentiation protocol with high efficiency and good reproducibility, which was a prerequisite to meeting the cell quantity and quality thresholds of preclinical and translational research[13]. Previous studies by ourselves and others described protocols to generate pancreatic β cells from human pluripotent stem cells in which a near homogenous population of pancreatic fate-committed PDX1$^+$ progenitor cells could be obtained; however, challenges remained in the subsequent commitment of these progenitors to pancreatic β cells at high efficiency[15–19]. Therefore, we focused on optimizing the differentiation protocol from pancreatic progenitor commitment to β cell fate decision by modulating signaling pathways and reconstructing spatial structure of islets. To generate pancreatic β cells, we used human induced pluripotent stem cell lines generated from a chemical reprogramming approach[20,21], which used extrinsic chemical stimulation to manipulate cell fate

[1]MOE Engineering Research Center of Regenerative Medicine, School of Basic Medical Sciences, State Key Laboratory of Natural and Biomimetic Drugs, Peking University Health Science Center and the MOE Key Laboratory of Cell Proliferation and Differentiation, College of Life Sciences, Peking-Tsinghua Center for Life Sciences, Peking University, Beijing, China. [2]Hangzhou Reprogenix Bioscience, Hangzhou, China. [3]Organ Transplant Center, NHC Key Laboratory for Critical Care Medicine, Tianjin First Central Hospital, Nankai University, Tianjin, China. [4]Institute of Medical Biology, Chinese Academy of Medical Sciences and Peking Union Medical College, Yunnan, China. [5]School of Life Sciences, Center for Bioinformatics, Peking University, Beijing, China. [6]Hangzhou Repugene Technology, Hangzhou, China. [7]Center for Quantitative Biology, Peking-Tsinghua Center for Life Sciences, Peking University, Beijing, China. [8]State Key Laboratory of Cell Biology, Shanghai Institute of Biochemistry and Cell Biology, Center for Excellence in Molecular Cell Science, Chinese Academy of Sciences, University of Chinese Academy of Sciences, Shanghai, China. [9]State Key Laboratory of Medical Molecular Biology, Department of Molecular Biology and Biochemistry, Institute of Basic Medical Sciences, Medical Primate Research Center, Neuroscience Center, Chinese Academy of Medical Sciences, School of Basic Medicine, Peking Union Medical College, Beijing, China. [10]These authors contributed equally: Yuanyuan Du, Zhen Liang, Shusen Wang, Dong Sun, Xiaofeng Wang, Liew Soon Yi, Shuaiyao Lu. ✉e-mail: zhongyangshen@vip.sina.com; pengxiaozhong@pumc.edu.cn; hongkui_deng@pku.edu.cn

by exposing the somatic cells to small molecules alone, designated hCiPSCs (Supplementary Fig. 1). We found that two factors were critical to generating β cells in vitro. First, the formation of dense, three-dimensional cell aggregates of posterior foregut-committed cells facilitated the efficient generation of NKX6.1$^+$C-peptide$^+$ cells (Extended Data Fig. 1a). Second, the small molecule combination of ISX9 (NeuroD1 inducer)[22] and Wnt-C59 (WNT inhibitor) at Stage 5 synergistically promoted the terminal differentiation of pancreatic endocrine progenitors (Extended Data Fig. 1b). With this optimized protocol, we were able to generate relatively uniform, islet-sized aggregates, containing NKX6.1$^+$C-peptide$^+$ cells at an efficiency of up to approximately 70% from hCiPSCs (Fig. 1a,b). Dynamic analysis of the differentiation process showed that approximately 90% of PDX1$^+$ pancreatic progenitors were generated by early Stage 4, which finally gave rise to 90% of CHGA$^+$NGN3$^-$ endocrine cells in Stage 6 (Extended Data Fig. 1c). Notably, the protocol showed stable performance, consistently reproducing similar results across differentiation batches (Supplementary Table 1). Collectively, these data indicated the establishment of a protocol that robustly promoted pancreatic endocrine differentiation from hCiPSCs.

We then characterized the hCiPSC-derived pancreatic endocrine cells in vitro. qRT–PCR showed similar expression levels of pancreatic genes in hCiPSC-derived pancreatic endocrine cells and human islets, and immunofluorescence staining confirmed that most C-peptide$^+$ cells co-expressed pancreatic transcription factors (Extended Data Fig. 1d,e). Notably, the expression of MAFA and UCN3, markers of mature β cells, was detected in hCiPSC-derived β cells (Extended Data Fig. 1d–g). We then analyzed the insulin secretion of hCiPSC-derived pancreatic β cells in comparison with human islets. In both static and dynamic assays, hCiPSC-derived pancreatic β cells showed insulin secretion in response to glucose challenges (Extended Data Fig. 2a,b), and these results were confirmed by glucose-stimulated calcium flux assay (Extended Data Fig. 2c). Immunoelectron microscopy confirmed the monohormonal feature of most hCiPSC-derived β cells, and dense-core, crystallized insulin granules were observed within these cells (Extended Data Fig. 2d–f).

In addition to β cells, we also identified glucagon (GCG)$^+$ α-like cells and somatostatin (SST)$^+$ δ-like cells in the aggregates (Fig. 1c). Flow cytometry analysis revealed that the final stage cell aggregates contained approximately 60% β cells, 11% α-like cells and 7% δ-like cells on average (Fig. 1d and Supplementary Fig. 2). Single-cell RNA sequencing analysis of S6D2 clusters confirmed the existence of the three major pancreatic endocrine cell populations (β cells, α-like cells and δ-like cells) and their proportions, which altogether accounted for 80%, and also revealed that the remaining approximately 20% of cells comprised pancreatic progenitors (~4%), proliferative endocrine cells (~2%) and enterochromaffin cells (~15%), a type of enteroendocrine cell that was also generated in β cell differentiation conditions reported by other groups[19,23] (Supplementary Fig. 3a–d). The expression of α-cell-specific genes was confirmed by qRT–PCR (Supplementary Fig. 3e). Moreover, typical glucagon secretory granules could be detected by electron microscopy, and glucagon secretion in the final stage aggregates was suppressed upon glucose challenge (Extended Data Fig. 2d–f and Supplementary Fig. 3f). Accordingly, these functional aggregates were designated hCiPSC-islets.

We further validated the function of hCiPSC-islets on a routinely used immunodeficient mouse model. After transplantation under the kidney capsule of streptozotocin (STZ)-induced diabetic mice, hCiPSC-islets survived with marked vascularization and preserved cellular complexity, shown by the presence of C-peptide$^+$ β cells, GCG$^+$ α-like cells and SST$^+$ δ-like cells 16 weeks post-transplantation (wpt) (Fig. 1e and Extended Data Fig. 3a–c). Fasting blood glucose levels of transplanted mice were restored to physiological levels, accompanied by increase in body weights (Fig. 1f and Extended Data Fig. 3d). Glucose tolerance tests showed glucose-responsive human C-peptide secretion as well as rapid glucose clearance (Fig. 1g and Extended Data Fig. 3e). Notably, the 15-week survival rate of hCiPSC-islet transplanted diabetic mice was over 85%, compared to less than 20% in the non-transplanted control group (Extended Data Fig. 3f). Fasting human C-peptide secretion increased steadily from 2 wpt to 12 wpt, after which it was maintained at around 1 ng ml^{-1} for up to 36 wpt in non-diabetic mice (Fig. 1h). The progressive increase of human C-peptide secretion in mouse plasma suggested continued maturation of the hCiPSC-islets after transplantation. Single-cell RNA sequencing analysis of kidney grafts at 10 wpt confirmed the functional maturation of all three pancreatic endocrine cell types and also revealed unaltered cell composition after transplantation (Supplementary Figs. 3–5). Notably, hierarchical clustering of S6D2 hCiPSC-islets, 10-wpt kidney grafts and primary human islets showed that the hCiPSC-differentiated pancreatic endocrine cells shared similar global gene expression profiles to their native counterparts in primary human islets (Fig. 1i,j). These data suggested the stable and long-term functionality of transplanted hCiPSC-islets in the mouse model.

Furthermore, the established protocol demonstrated good compatibility across cell lines, as shown by reproduction of similar in vitro characteristics and in vivo functionality on hCiPSC-islets derived from another three independent hCiPSC cell lines (Extended Data Fig. 4a–d and Supplementary Table 1). Notably, in all hCiPSC-islets transplanted mice, no tumorigenesis was observed ($n=190$). The observation period of hCiPSC-islets transplanted mice was up to 48 weeks, and immunofluorescence staining of the kidney graft showed not only that the three major pancreatic endocrine cell types were maintained in the transplanted hCiPSC-islets but also that they matured in vivo, with a high proportion of β cells and α cells expressing UCN3 (Extended Data Fig. 4e,f). Collectively, these results indicated that long-term survival and function of transplanted hCiPSC-islets was well replicated on multiple hCiPS cell lines. The demonstration of the safety and efficacy of hCiPSC-islets in the mouse model laid the groundwork for research in non-human primates.

Fig. 1 | hCiPSC-derived islets generated in vitro resemble primary human islets and reverse diabetes in mice. a, Schematic of the hCiPSC-islet differentiation protocol. **b**, Left: representative bright-field image of Stage 6 cell aggregates. Scale bar, 500 μm. Right: representative flow cytometry analysis of the expression of β cell markers in Stage 6 aggregates. **c**, Representative immunofluorescence staining of islet hormones in sectioned Stage 6 aggregates. Scale bar, 50 μm. **d**, Proportions of islet hormone$^+$ cells in Stage 6 aggregates detected by flow cytometry ($n=6$). **e**–**h**, In vivo characterization of hCiPSC-islets. **e**, Immunofluorescence staining of islet hormones and key markers of β cells in hCiPSC-islet graft at 16 wpt. Scale bar, 50 μm. **f**, Fasting blood glucose levels of hCiPSC-islet transplanted diabetic mice ($n=22$). **g**, Human C-peptide secretion in response to glucose challenge in hCiPSC-islet transplanted mice at 16 wpt ($n=17$ animals measured at two technical replicates each). Stimulation indices as indicated above bars. **h**, Continuous detection of fasting human C-peptide secretion in hCiPSC-islet transplanted non-diabetic mice; first detection was conducted at 2 wpt ($n=31$). **i, j**, Single-cell RNA sequencing of hCiPSC-islets and human islets. **i**, Hierarchical clustering of global gene expression profiles of cell types present in hCiPSC-islets generated in vitro (hCiPSC-islets_S6D2), hCiPSC-islet grafts at 10 wpt in mice (hCiPSC-islets_10 wpt) and cell types present in primary human islets (human islets). **j**, Superimposed UMAP projections of hCiPSC-islets_S6D2, hCiPSC-islets_10 wpt and human islets. Datasets are colored according to their assigned cell identity. Data are presented as mean values ± s.e.m. UMAP, uniform manifold approximation and projection.

Next, we investigated the efficacy and safety of hCiPSC-islet transplantation in a non-human primate model. Four healthy adult rhesus macaques (*Macaca mulatta*) (Monkeys 1–4) were used for long-term observation (Supplementary Table 3). All four macaques developed diabetes after a single high-dose STZ injection, resulting in fasting blood glucose levels of over 200 mg dl^{-1} and C-peptide levels lower than 0.15 ng ml^{-1} (0.09 ± 0.03 ng ml^{-1}) (Figs. 2a–d and 4a–d)[24]. Administration of exogenous insulin was initiated 3 d after the STZ injection. The exogenous insulin requirement of the four diabetic recipients ranged between 2 and 4 IU kg^{-1} per day (2.89 ± 0.58 IU kg^{-1} per day) at 1 week before cell transplantation, which was similar to previous reports (Fig. 3a–d)[24–26]. Although

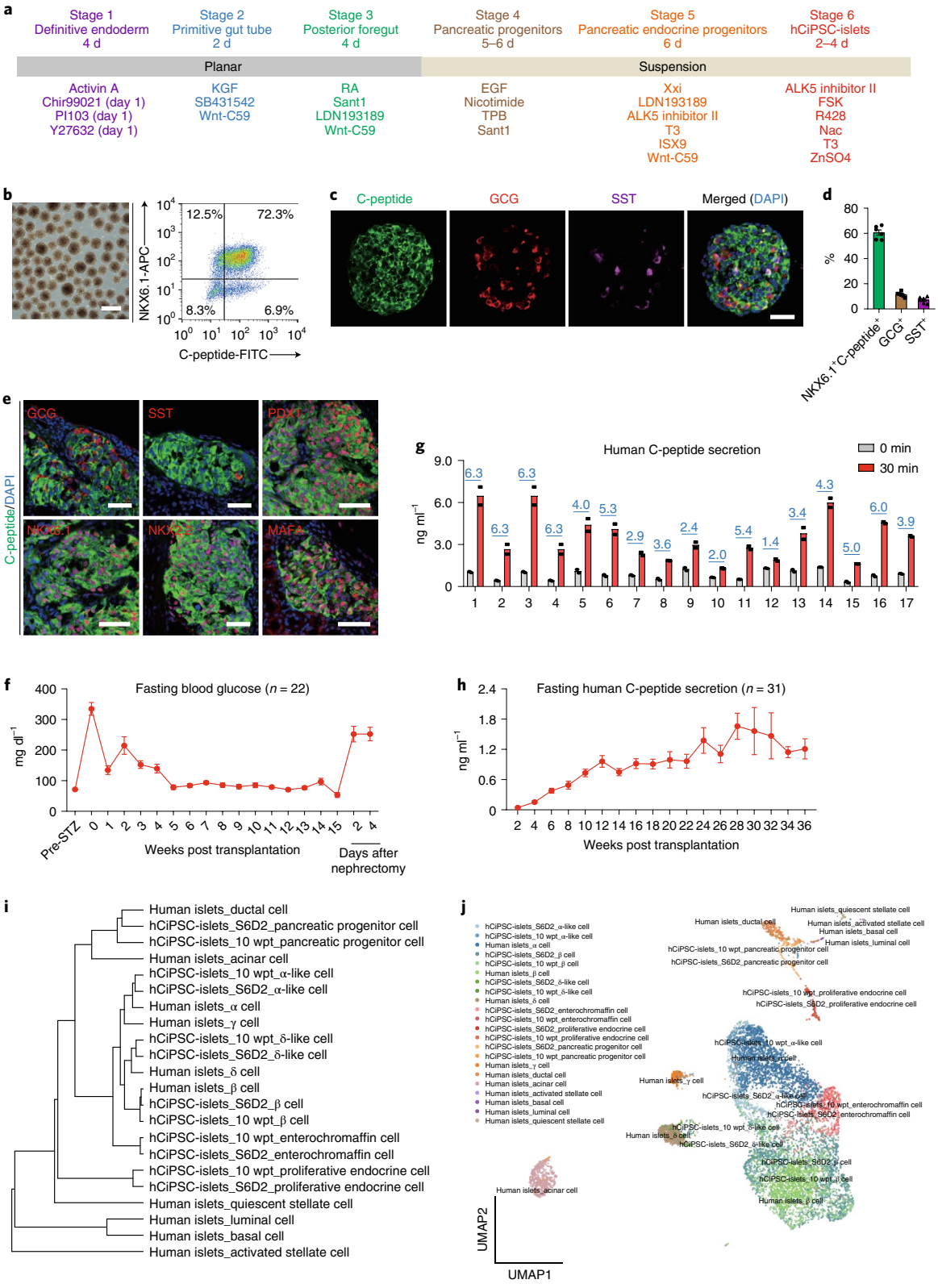

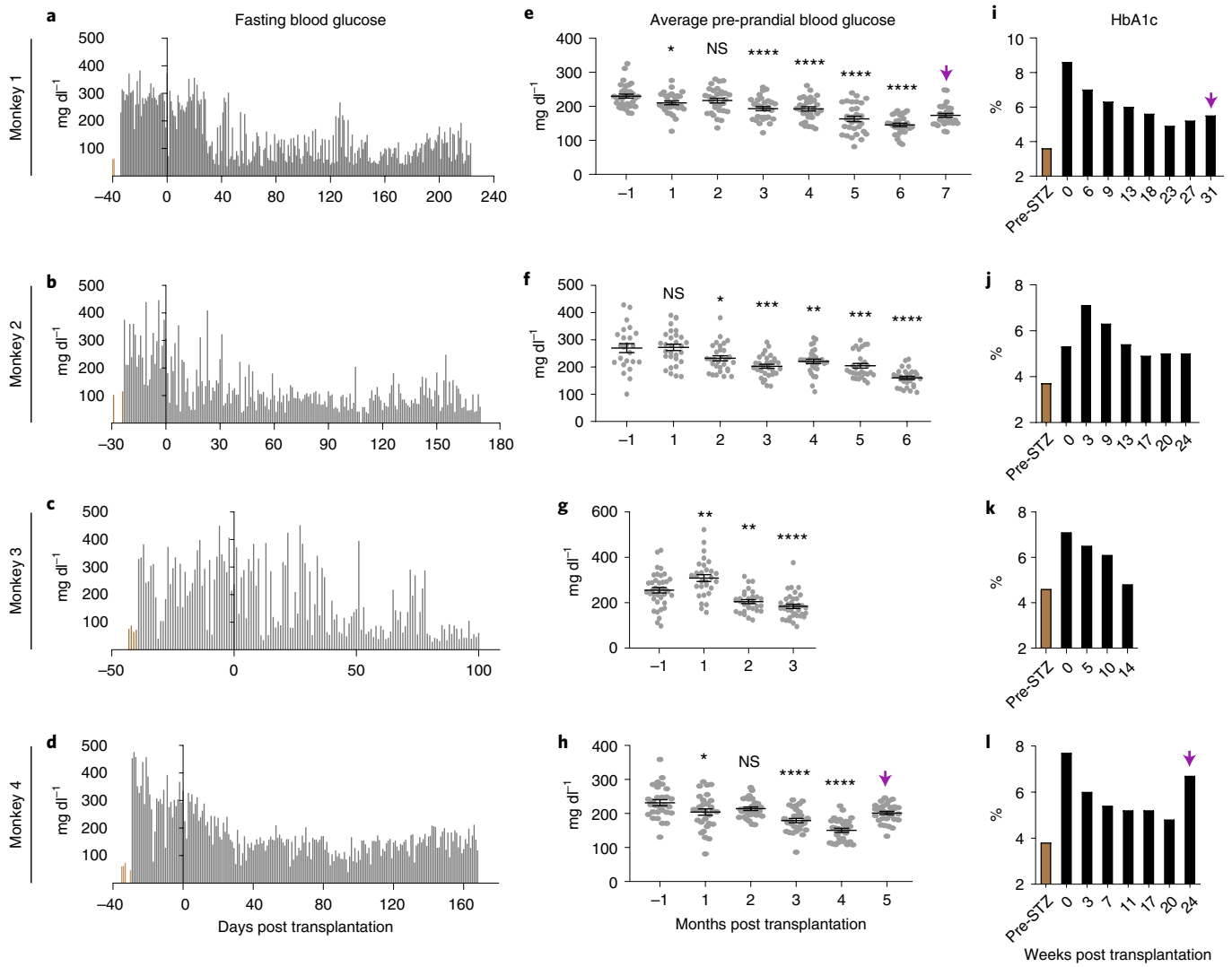

Fig. 2 | Intraportal infusion of hCiPSC-islets led to improvement of glycemic control in immunosuppressed diabetic rhesus macaques. Long-term tracking of glycemic measures in diabetic Monkey 1 (**a**, **e**, **i**), Monkey 2 (**b**, **f**, **j**), Monkey 3 (**c**, **g**, **k**) and Monkey 4 (**d**, **h**, **l**) before and after infusion of hCiPSC-islets. **a**–**d**, Daily fasting blood glucose levels of the monkeys before and after infusion of hCiPSC-islets (infusion procedure conducted at day 0). Fasting blood glucose levels before diabetes induction are indicated in brown. **e**–**h**, Average pre-meal blood glucose levels of the monkeys before and after infusion of hCiPSC-islets. A change in trend of pre-meal blood glucose levels at the 7th and 5th month after transplant in Monkeys 1 and 4 suggests possible graft failure (purple arrows). Each data point represents averaged value of three daily pre-prandial blood glucose levels. At pre-transplant (−1 month), $n = 24$, 34, 39 and 29 daily pre-prandial blood glucose values, respectively, for Monkeys 1–4; for the final month after transplantation, $n = 29$, 30, 36 and 30, respectively, for Monkeys 1–4; for post-transplant months in between, $n = 30$ in all monkeys. Unpaired two-tailed t-test was used to determine significance in each group from pre-infusion (−1 month) levels. P values for Monkey 1 for each month after transplantation are as follows: 0.0171, 0.1540 and <0.0001 for months 3–6. P values for Monkey 2 for each month after transplantation: 0.8939, 0.0413, 0.0002, 0.0067, 0.0005 and <0.0001. P values for Monkey 3 for each month after transplantation: 0.0064, 0.0020 and <0.0001. P values for Monkey 4 for each month after transplantation: 0.0375, 0.0848 and <0.0001 for months 3–4. $^{*}P < 0.05$, $^{**}P < 0.005$, $^{***}P < 0.0005$ and $^{****}P < 0.00005$. NS, not significant. Data are presented as mean values ± s.e.m. **i**–**l**, Glycated hemoglobin (HbA1c) levels of the monkeys before diabetes induction (indicated in brown), before infusion (0 wpt) and after infusion of hCiPSC-islets. Re-elevation of HbA1c levels (purple arrows) suggests possible graft failure.

all macaques were treated with intensive insulin therapy, levels of glycated hemoglobin A1c (HbA1c) substantially increased from 3.9 ± 0.5% to 7.2 ± 1.4% within 1–2 months after STZ injection, indicating a rapid progression of diabetes (Fig. 2i–l). Notably, we observed that Monkey 3 exhibited characteristics of labile diabetes, shown by swings in blood glucose levels that ranged from 40 mg dl^{-1}to 545 mg dl^{-1} within a day and also fasting blood glucose levels that ranged from 40 mg dl^{-1} to 450 mg dl^{-1} before cell transplantation (Fig. 2c)[27,28].

To protect the human grafts, immunosuppressive therapy was administered 9 d before transplantation, following a protocol designed based on previous studies of islet xenotransplantation into non-human primates (Supplementary Fig. 6a)[25,26]. In brief, to achieve long-term immunosuppression, induction immunosuppression was applied, in which both B cells and T cells were depleted (Supplementary Fig. 6b); immunosuppression was maintained using tacrolimus and sirolimus and biweekly treatment with belatacept (Supplementary Fig. 6a,c).

To produce a ready-to-use cell source for macaque transplantation, we optimized a cryopreservation and recovery protocol for hCiPSC-islets. After generation, hCiPSC-islets were cryopreserved at single cell and then recovered and reaggregated 2 d before

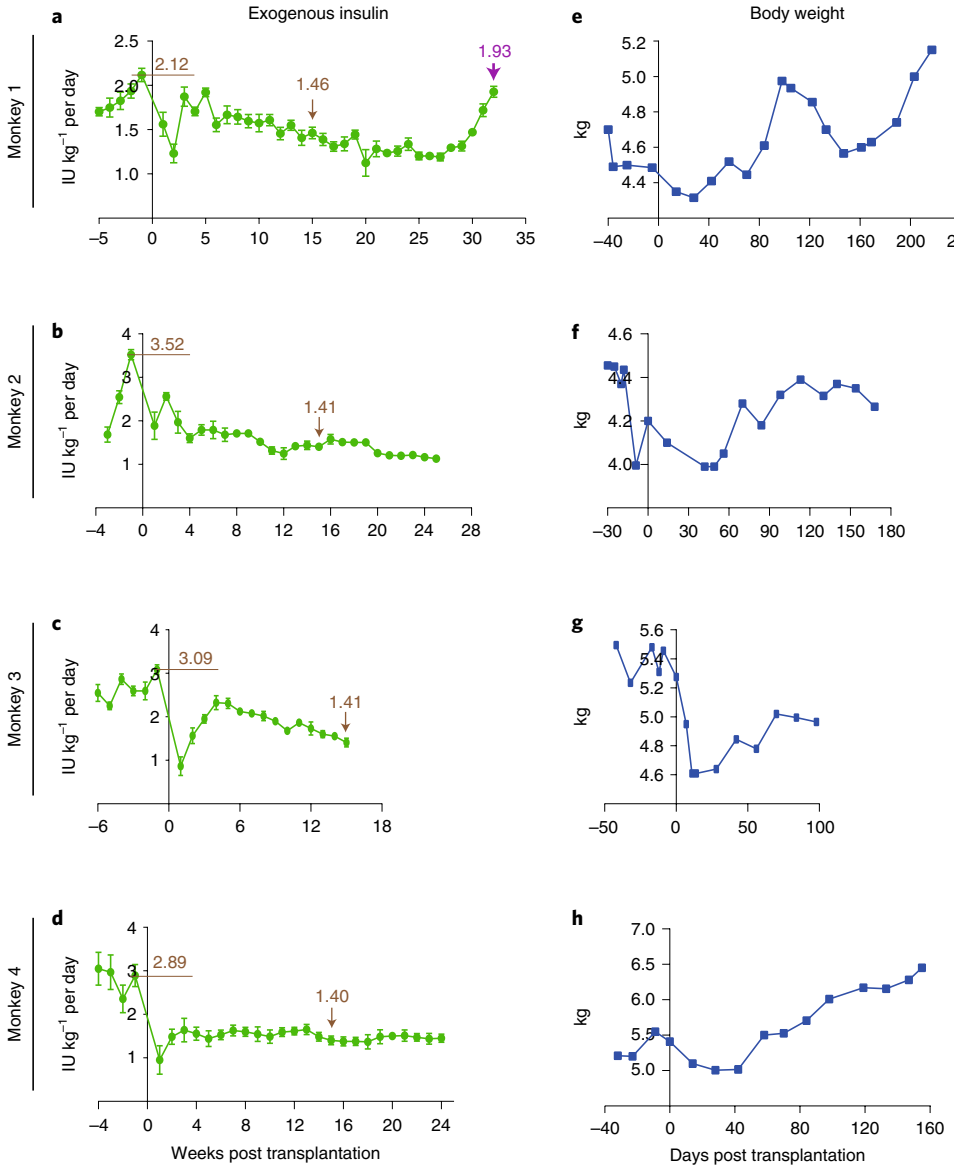

Fig. 3 | hCiPSC-islet transplanted diabetic macaques showed significant reduction of exogenous insulin requirement and overall increase of body weight. Long-term tracking of exogenous insulin requirements and body weights in diabetic Monkey 1 (**a**, **e**), Monkey 2 (**b**, **f**), Monkey 3 (**c**, **g**) and Monkey 4 (**d**, **h**) before and after infusion of hCiPSC-islets. **a**–**d**, Weekly average exogenous insulin dose. Exogenous insulin requirement at the last week before infusion and at 15 wpt are indicated in brown. Each data point represents weekly value based on averaged daily exogenous insulin doses ($n=7$ independent dose values). Re-elevation of exogenous insulin requirement in Monkey 1 at 33 wpt suggests possible graft failure (purple arrow). Data are presented as mean values ± s.e.m. **e**–**h**, Tracking of body weights of the monkeys.

infusion. The average viability and yield of hCiPSC-islets after recovery were 86.9% ± 1.6% and 82.0% ± 9.5%, respectively (Supplementary Table 3). The detailed pre-transplantation characterization of hCiPSC-islets is described in Supplementary Table 3.

Recovered hCiPSC-islets were transplanted into the diabetic macaques at a single dose by intraportal infusion. The dose of hCiPSC-islets transplanted was designed based on previously reported dosing for adult pig islets to monkey xenotransplantation[29–32]. In this study, hCiPSC-islets were infused at a dose ranging from 32,000 islet equivalents (IEQ) kg^{-1} to 45,100 IEQ kg^{-1} and of about 39,600 IEQ kg^{-1} on average (Supplementary Tables 2 and 3). The increased IEQ requirement in a xenotransplantation setting relative to clinical islet transplantation was mainly due to species incompatibilities and metabolic differences[33]. After hCiPSC-islet infusion, transient liver injury was detected, a phenomenon also observed in clinical intraportal islet transplantation[8,34]; however, all recipients recovered after administration of liver protective drug (Supplementary Table 4). Notably, all four recipients exhibited relief from diabetic symptoms after hCiPSC-islet transplantation (Figs. 2 and 3). Firstly, fasting blood glucose levels decreased and stabilized over time (Fig. 2a–d), especially in Monkey 4, in which an obvious a downward trend was observed in the first month after transplantation (Fig. 2d). Secondly, the average pre-prandial blood glucose levels were also significantly decreased in all recipients after hCiPSC-islet infusion (Fig. 2e–h). Accordingly, HbA1c, a universal clinical measurement for glycemic control in patients with diabetes[35,36], decreased from 7.2 ± 1.4% before transplantation to 5.4 ± 0.5% at 3 months after transplantation on average (Fig. 2i–l). Notably, these improvements were also seen in Monkey 3, the recipient exhibiting a labile diabetes-like state after STZ

injection (Fig. 2c,g,k). Collectively, our results revealed that transplantation of hCiPSC-islets effectively lowered hyperglycemia and improved overall glycemic control in all diabetic macaques.

Furthermore, the exogenous insulin requirement substantially decreased after hCiPSC-islet transplantation (Fig. 3a–d). At 1–2 weeks after hCiPSC-islet infusion, a dip in exogenous insulin requirement was seen in all recipients, which was likely due to decreased appetite in the recovery period after surgery and intense immunosuppression around the time of transplantation. Exogenous insulin requirement increased upon recovery to a normal diet. As hCiPSC-islets engrafted and matured in vivo, exogenous insulin requirement gradually decreased and stabilized over time. At 15 weeks after hCiPSC-islets infusion, exogenous insulin requirement in the four recipients decreased by 31% (from 2.12 IU kg^{-1}per day to 1.46 IU kg^{-1} per day), by 60% (from 3.52 IU kg^{-1}per day to 1.41 IU kg^{-1} per day), by 54% (from 3.09 IU kg^{-1} per day to 1.41 IU kg^{-1} per day) and by 52% (from 2.89 IU kg^{-1} per day to 1.40 IU kg^{-1} per day), respectively, compared to pre-transplant levels (Fig. 3a–d). Moreover, body weights of recipient macaques increased after 6 weeks after hCiPSC-islet infusion (Fig. 3e–h).

C-peptide secretion was continuously monitored in all macaques. We observed a gradual increase of secreted C-peptide levels in all recipients within the first 1–2 months after hCiPSC-islet infusion, suggesting a functional maturation of hCiPSC-islets in vivo (Fig. 4a–d). Furthermore, C-peptide secretion responded to meal challenges starting from 4 wpt to 8 wpt in all recipients (Fig. 4e–h). In Monkey 2, the fold changes in post-prandial C-peptide levels over fasting levels exceeded 3 from 8 wpt to 16 wpt (Fig. 4f). The level of C-peptide secretion peaked within 8 wpt, with an average secretion level of 0.37 ± 0.29 ng ml^{-1} at 8 wpt, a marked increase from pre-transplantation levels (0.09 ± 0.03 ng ml^{-1}) (Fig. 4e–h). The significant increase of secreted C-peptide levels in all recipients was consistent with the observed improvement in glycemic control and decreased exogenous insulin requirements.

After an extended period of time, at 5–6 months after transplant, hCiPSC-islet graft failure was observed on Monkey 1 and Monkey 4. For Monkey 1, the exogenous insulin requirement substantially increased at 6 months after hCiPSC-islets transplantation, which was accompanied by rises in pre-prandial blood glucose and HbA1c (Figs. 2e,i and 3a). For Monkey 4, a significant increase of HbA1c (from 4.8% to 6.7%) and a rise in pre-prandial blood glucose was observed at 5 months after infusion, although exogenous insulin dose requirement did not markedly increase (Fig. 2h,l and 3d). Monkey 1 and Monkey 4 were euthanized after human graft failure for further analysis.

For Monkey 2, post-transplant lymphoproliferative disorder (PTLD) was diagnosed at 176 days post-transplantation (dpt), and it was subsequently euthanized at 180 dpt (Supplementary Table 5). For Monkey 3, hematochezia was observed at 100 dpt, and the monkey died of massive colon hemorrhage at 101 dpt. These two severe adverse events might have occurred as side effects of intensive immunosuppression, which was previously reported[37–39]. Full necropsy was conducted on all four recipients after death or euthanasia. Postmortem examinations revealed no macroscopic and microscopic evidence of tumorigenesis after hCiPSC-islets transplantation (Extended Data Fig. 5).

To confirm that the improved glycemic control seen in the recipient macaques was due to transplanted hCiPSC-islets, we conducted postmortem histological analysis on the native pancreata of Monkeys 1–4 (Extended Data Fig. 6). Histological analysis showed that the structure of native islets was destroyed, and native β cells were specifically eliminated by STZ, as indicated by the very rare occurrence of C-peptide$^+$ cells in the remaining islets; in particular, C-peptide$^+$ cells were almost undetectable in Monkey 3 (Extended Data Fig. 6). Most studies have reported that β cell regeneration did not occur in macaques after STZ treatment[24,40–42], and one study showed that the emergence of CK19$^+$Proinsulin$^+$ co-expressing cells could indicate the regeneration of endogenous β cells in pancreas after STZ treatment[43]. In all four analyzed monkeys, CK19$^+$Proinsulin$^+$ cells were not detected (Supplementary Fig. 7), suggesting the absence of β cell regeneration after STZ treatment, which is consistent with most reports[24,40–42]. Collectively, these findings indicated the severe destruction of native β cells, with no sign of β cell recovery in the pancreas of the recipient macaques.

We also performed postmortem histological analysis of livers of all four macaques. hCiPSC-islet grafts were found residing in the portal vein of Monkey 3 (Fig. 4i). As anticipated, no hCiPSC-islet grafts were detected in Monkey 1 and Monkey 4. In Monkey 2, a severe lymphocyte infiltration was observed in the liver (Extended Data Fig. 5d), and the intraportal hCiPSC-islets were not detected, possibly due to destruction by infiltrating immune cells after onset of PTLD. We further confirmed the intraportal grafts in Monkey 3 derived from hCiPSC-islet infusion by immunofluorescence staining of Stem121 (a human cell marker) (Fig. 4i). The results also showed that the intraportal hCiPSC-islets contained C-peptide$^+$ cells, which co-expressed with other β cell markers, including PDX1, NKX6.1 and NKX2.2 (Fig. 4i). Additionally, GCG$^+$ α cells were also detectable in hCiPSC-islet grafts, which did not express β cell markers PDX1 and NKX6.1 (Extended Data Fig. 7a). Combined with the findings in the pancreas, our data suggest that the amelioration of diabetes observed in recipient macaques resulted from hCiPSC-islet transplantation.

Further characterization of the intraportal hCiPSC-islet grafts in Monkey 3 revealed that, compared to pre-transplant levels, the proportion of C-peptide$^+$ cells in intraportal hCiPSC-islets had decreased (Extended Data Fig. 7b and Supplementary Table 3). These observations of graft loss and decreased C-peptide in the diabetic macaques was in contrast with what was observed in the immunodeficient mouse model, in which the cellular composition before and after transplantation was almost unchanged, and β cells were well maintained (Fig. 1e, Supplementary Figs. 3b and 4b and Extended Data Fig. 4f). Considering that many studies showed the occurrence of chronic immune attack leading to progressive graft loss in allogenic and xenogeneic transplants[9,26], we analyzed immune cell infiltration of the intraportal hCiPSC-islet grafts. The results showed the presence of CD3$^+$ T cells and CD68$^+$ macrophages in the periphery of and inside the hCiPSC-islets, whereas CD20$^+$ B cells were rarely observed inside the human graft (Extended Data Fig. 7c). These data suggest the occurrence of immune attack against xenografts in this immunosuppressed macaque model, which could be the underlying reason for the reduction in C-peptide secretion over time after hCiPSC-islet infusion (Fig. 4a–h).

Fig. 4 | Detection of secreted C-peptide in hCiPSC-islet transplanted diabetic rhesus macaques. Long-term tracking of C-peptide secretion in diabetic Monkey 1 (**a**, **e**), Monkey 2 (**b**, **f**), Monkey 3 (**c**, **g**) and Monkey 4 (**d, h**) before and after infusion of hCiPSC-islets. **a**–**d**, Random C-peptide levels of the transplanted monkeys before diabetes induction (brown), before infusion (0 wpt) and after infusion ($n = 3$ technical replicates). **e**–**h**, Fasting and post-prandial C-peptide secretion in the transplanted monkeys ($n = 3$ technical replicates). Decline of secreted C-peptide and reduction of glucose-stimulated C-peptide response index suggest possible graft failure (purple arrows). Data are presented as mean values ± s.e.m. **i**, Immunofluorescence staining of Stem121, islet hormones and β cell transcription factors in representative liver sections of Monkey 3 at 101 d after transplantation. Scale bar, 50 μm. Magnified images of boxed areas shown on the right. Scale bar, 20 μm.

To further confirm that the improvements in glycemic control observed in Monkeys 1–4 were the result of hCiPSC-islet transplantation, a fifth STZ-induced macaque (Monkey 5) was added to this study. Different from the first four monkeys, which were transplanted with hCiPSC-islets within 1–2 months after STZ injection, Monkey 5 received insulin therapy for nearly half a year after STZ

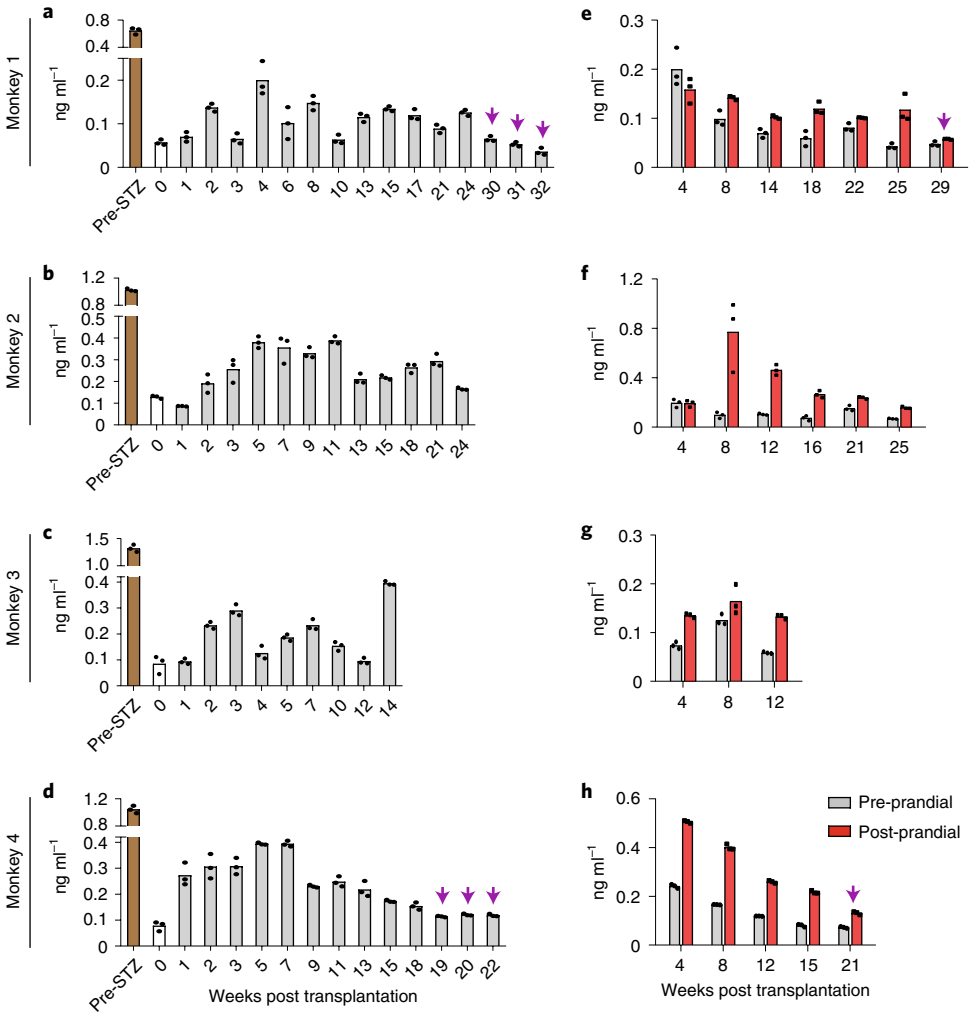

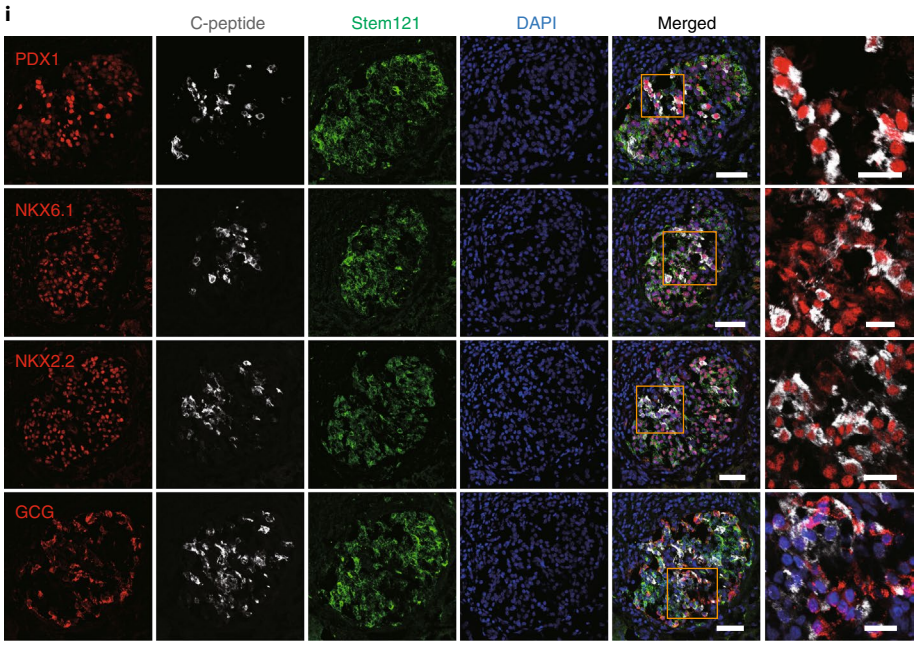

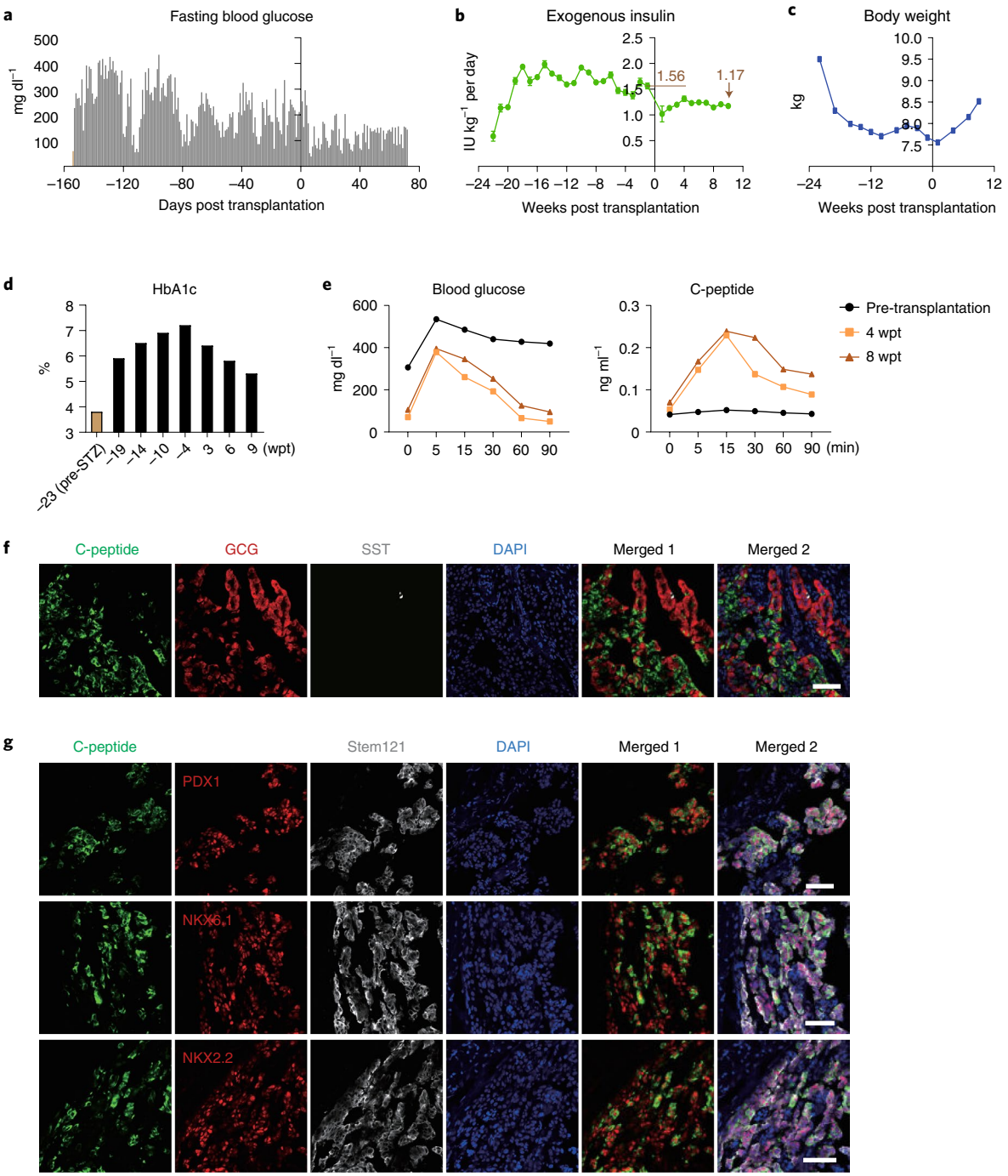

Fig. 5 | Amelioration of diabetes by intrahepatic infusion of hCiPSC-islets into a macaque (Monkey 5), which was treated with exogenous insulin for 6 months after STZ injection. a, Daily fasting blood glucose levels of Monkey 5 before and after infusion of hCiPSC-islets (infusion performed at day 0). **b**, Weekly average exogenous insulin dose. Exogenous insulin requirement at the last week before infusion and at 10 wpt are indicated in brown. Each data point represents weekly value based on averaged daily exogenous insulin doses ($n = 7$ independent dose values). Data are presented as mean values ± s.e.m. **c**, Tracking of body weight of Monkey 5. **d**, HbA1c levels of Monkey 5 before diabetes induction (indicated in brown), before infusion and after infusion of hCiPSC-islets. **e**, Blood glucose levels (left; $n = 2$ technical replicates) and C-peptide secretion (right; $n = 3$ technical replicates) in response to glucose challenge in Monkey 5 before and after transplantation. **f**, Representative immunofluorescence staining of islet hormones in intrahepatic hCiPSC-islet grafts in Monkey 5 liver sections. Scale bar, 50 μm. **g**, Representative immunofluorescence staining of key β cell markers and Stem121 in intrahepatic hCiPSC-islet grafts in Monkey 5 liver sections. Scale bar, 50 μm.

treatment without cell transplantation (Fig. 5). Throughout this time, HbA1c level of Monkey 5 progressively increased (reaching 7.2% 19 weeks after STZ treatment); exogenous insulin requirement remained high; and body weight continuously decreased (Fig. 5a–d). Notably, the C-peptide level remained extremely low and showed no responsiveness to glucose challenge (Fig. 5e). These data indicate that exogenous insulin administration alone or residual β cells after STZ treatment did not confer adequate glycemic control

in diabetic Monkey 5. After hCiPSC-islet transplantation, Monkey 5 exhibited improved glycemic results similar to Monkeys 1–4, with a significant reduction of HbA1c to 5.3% over 9 weeks after infusion, accompanied by a reduction of exogenous insulin requirement and increase of body weight (Fig. 5a–d). Moreover, the intravenous glucose tolerance test (IVGTT) showed that glucose clearance capacity was substantially improved after transplantation (Fig. 5e), and an obvious C-peptide secretion peak could be detected upon both glucose and arginine challenges (Fig. 5e and Extended Data Fig. 8a). The monkey was euthanized at 10 wpt, and a full autopsy showed no evidence of teratoma or other tumor formation (Extended Data Fig. 8b,c). Immunofluorescence staining of liver sections showed that the intraportal grafts of Monkey 5 contained C-peptide$^+$ β cells, GCG$^+$ α cells and SST$^+$ δ cells (Fig. 5f,g). Collectively, these data confirmed the findings that hCiPSC-islet transplantation improved glycemic control in the diabetic macaque recipients.

Similarly to Monkey 3, the proportion of β cells in the intraportal hCiPSC-islets of Monkey 5 also decreased at 10 wpt in contrast to that before infusion (Extended Data Fig. 8h). Therefore, we conducted single-cell RNA sequencing analysis on peripheral blood mononuclear cells (PBMCs) of Monkey 5 to analyze the potential immune response of recipient macaque to hCiPSC-islets. A profound depletion of T cells, B cells and natural killer (NK) cells was observed after administration of immunosuppressants; however, these cell populations gradually recovered after hCiPSC-islets infusion (Supplementary Fig. 8b). The proportion of T cells and NK cells returned to pre-immunosuppression levels at 4 wpt (Supplementary Fig. 8b), whereas, in B cells, gene expression pattern was substantially altered after hCiPSC-islets infusion. Genes upregulated in B cells at 8 wpt were mainly enriched in immunoreactivity, such as adaptive immune response and B cell proliferation (Supplementary Fig. 8c). Similar changes of gene expression pattern were observed in NK cells (Supplementary Fig. 8c). In addition, further analysis showed the adaptive immune response to hCiPSC-islets in Monkey 5 in terms of complement deposition and T cell infiltration into the hCiPSC-islet grafts, the generation of donor-specific antibodies as well as the detection of complement dependent cytotoxicity and robust IFN-γ secretion when PBMCs of Monkey 5 were incubated with hCiPSC-islets in vitro (Extended Data Fig. 9). The immune attack against human grafts could have led to the generation of a population of PDX1$^+$NKX6.1$^+$C-peptide$^-$ cells in the monkey liver grafts (Figs. 4i and 5g and Extended Data Fig. 10), in which PDX1 expression was observed to be relatively lower. This decrease in PDX1 expression might have resulted in the loss of insulin expression in this subpopulation (Figs. 4i and 5g and Extended Data Fig. 10a). PDX1 has been reported as one of the most important regulators of insulin expression[44,45], and its expression could be significantly repressed by factors like inflammatory factors (such as IFN-γ and IL1-β)[46,47] and commonly used immunosuppressants (such as tacrolimus)[48]. Collectively, these results showed that, even under the severe immunosuppression regimen, immune attack against the human grafts occurred after hCiPSC-islet transplantation and led to graft failure, which suggests that the appropriate rejection prophylaxis to protect hCiPSC-islet grafts could be important to maximizing clinical benefit of hPSC-islet transplantation.

Discussion

In this study, we established a differentiation protocol to generate islets from human pluripotent stem cells with high efficiency and stability, whose generated islets showed similar global gene expression patterns to that of human islets, robust expression of mature islet markers such as MAFA and UCN3 as well as biphasic insulin secretion. We show that these hPSC-islets are able to relieve hyperglycemia and improve overall glycemic control in a pre-clinical context. Firstly, transplantation of our hPSC-islets effectively decreased HbA1c and restored endogenous C-peptide secretion (Figs. 2–5), which are positive outcomes previously associated with control of disease progression[49,50]. Clinical studies have associated each percentage point reduction of HbA1c with profound reduction in risk of diabetic-related complications[51,52]. Additionally, the restoration of endogenous C-peptide has also been credited as the main factor associated with overall clinical benefit in clinical islet transplantation[7]. Secondly, we observed that one recipient macaque presenting the features of labile diabetes benefited from hPSC-islet transplantation (Fig. 2c,g,k). Clinical reports have shown strong evidence that refractory hypoglycemia, a predominantly life-threatening symptom in patients with 'brittle diabetes', can be resolved with clinical islet cell transplantation[5,28,53]. Although more animals should be tested, our data suggest the potential of hPSC-islet infusion in improving glycemic control and of correcting severe hypoglycemia in this selected group of patients with labile diabetes. Finally, the ability to be efficiently cryopreserved makes hCiPSC-islets a consistently available, ready-to-use cell source, which is especially important for clinical application and affords much-needed flexibility in transplantation into humans[54]. Collectively, these data suggest that, as a sustainable cell source, pluripotent stem-cell-derived islets hold great potential for clinical application and could bring benefits to patients with diabetes.

Furthermore, we found that certain factors could affect the in vivo functional capacity of hCiPSC-islets after transplantation. On the one hand, a favorable microenvironment to effectively support survival, maturation and maintenance of hCiPSC-islets was important for their functional capacity after transplantation. When transplanted into mice, a period of maturation was observed, as indicated by the gradual increase of C-peptide secretion for up to 12 weeks, and the function of hCiPSC-islets could be maintained long term (Fig. 1h and Extended Data Fig. 4d). By contrast, after transplantation into diabetic macaques, a marked increase in C-peptide secretion was observed in the first 1–2 months after transplantation (Fig. 4a–d); subsequently, however, in a distinct departure from the trends observed in the transplanted mice, C-peptide secretion could not be sustained and even decreased (Fig. 4b,d,f,h). Possible reasons that could have contributed to these phenomena include the severe immune attack on xenografts and potential side effects of immunosuppressants, which have been reported on primary human islets[7,9–12]. These results suggested the importance of establishing an adequate strategy to effectively protect hPSC-derived islets and facilitate their long-term function in vivo. On the other hand, although the transplantation dose of hCiPSC-islets was similar to xenotransplanted primary adult pig islets, the latter showed a better capacity for diabetes reversal in the macaque model, which indicated that hCiPSC-islets were less functional than primary islets. Combined with the results of in vitro characterization (Extended Data Fig. 2a–c), these data suggest that hCiPSC-derived pancreatic β cells did not fully recapitulate the functionality of primary human islets, and further improvement of the differentiation protocol to enhance the function of hCiPSC-islets and reinforce the internal control of hormone secretion could boost its therapeutic effect.

In addition, although no tumorigenesis was observed in any of the animals transplanted in our study, strategies to ensure the safety of subjects are worth continued research, because, under clinical settings, the increased transplanted cell number could increase the potential risk of teratoma formation, which would be of particular concern in immunosuppressed patients[55,56]. Therefore, continued efforts to develop strategies, such as the establishment of adequate safeguards and development of retrievable encapsulation devices, could be valuable to clinical application of hPSC-islets[57–61]. In summary, as the first comprehensive report, to our knowledge, on the long-term assessment of hCiPSC-islets in a primate model of diabetes, the data obtained in this study provide valuable insights for stem-cell-derived islets in clinical research for diabetes treatment.

Online content

Any methods, additional references, Nature Research reporting summaries, source data, extended data, supplementary information, acknowledgements, peer review information; details of author contributions and competing interests; and statements of data and code availability are available at https://doi.org/10.1038/s41591-021-01645-7.

Received: 10 January 2021; Accepted: 29 November 2021;
Published online: 3 February 2022

References

1. Sneddon, J. B. et al. Stem cell therapies for treating diabetes: progress and remaining challenges. *Cell Stem Cell* **22**, 810–823 (2018).
2. Nair, G. G., Tzanakakis, E. S. & Hebrok, M. Emerging routes to the generation of functional β-cells for diabetes mellitus cell therapy. *Nat. Rev. Endocrinol.* **16**, 506–518 (2020).
3. Harding, J. D. Nonhuman primates and translational research: progress, opportunities, and challenges. *ILAR J.* **58**, 141–150 (2017).
4. Katsarou, A. et al. Type 1 diabetes mellitus. *Nat. Rev. Dis. Prim.* **3**, 17016 (2017).
5. Vantyghem, M. C., de Koning, E. J. P., Pattou, F. & Rickels, M. R. Advances in β-cell replacement therapy for the treatment of type 1 diabetes. *Lancet* **394**, 1274–1285 (2019).
6. Shapiro, A. M. et al. Islet transplantation in seven patients with type 1 diabetes mellitus using a glucocorticoid-free immunosuppressive regimen. *N. Engl. J. Med.* **343**, 230–238 (2000).
7. Shapiro, A. M., Pokrywczynska, M. & Ricordi, C. Clinical pancreatic islet transplantation. *Nat. Rev. Endocrinol.* **13**, 268–277 (2017).
8. Rickels, M. R. & Robertson, R. P. Pancreatic islet transplantation in humans: recent progress and future directions. *Endocr. Rev.* **40**, 631–668 (2019).
9. Gibly, R. F. et al. Advancing islet transplantation: from engraftment to the immune response. *Diabetologia* **54**, 2494–2505 (2011).
10. Lacotte, S., Berney, T., Shapiro, A. J. & Toso, C. Immune monitoring of pancreatic islet graft: towards a better understanding, detection and treatment of harmful events. *Expert Opin. Biol. Ther.* **11**, 55–66 (2011).
11. Johnson, J. D. et al. Different effects of FK506, rapamycin, and mycophenolate mofetil on glucose-stimulated insulin release and apoptosis in human islets. *Cell Transplant.* **18**, 833–845 (2009).
12. Tanemura, M. et al. Rapamycin induces autophagy in islets: relevance in islet transplantation. *Transplant. Proc.* **41**, 334–338 (2009).
13. Blau, H. M. & Daley, G. Q. Stem cells in the treatment of disease. *N. Engl. J. Med.* **380**, 1748–1760 (2019).
14. Harding, J., Roberts, R. M. & Mirochnitchenko, O. Large animal models for stem cell therapy. *Stem Cell Res. Ther.* **4**, 23 (2013).
15. Rezania, A. et al. Reversal of diabetes with insulin-producing cells derived in vitro from human pluripotent stem cells. *Nat. Biotechnol.* **32**, 1121–1133 (2014).
16. Pagliuca, F. W. et al. Generation of functional human pancreatic β cells in vitro. *Cell* **159**, 428–439 (2014).
17. Liu, H. et al. Systematically labeling developmental stage-specific genes for the study of pancreatic β-cell differentiation from human embryonic stem cells. *Cell Res.* **24**, 1181–1200 (2014).
18. Hogrebe, N. J. & Augsornworawat, P. Targeting the cytoskeleton to direct pancreatic differentiation of human pluripotent stem cells. *Nat. Biotechnol.* **38**, 460–470 (2020).
19. Veres, A. et al. Charting cellular identity during human in vitro β-cell differentiation. *Nature* **569**, 368–373 (2019).
20. Hou, P. et al. Pluripotent stem cells induced from mouse somatic cells by small-molecule compounds. *Science* **341**, 651–654 (2013).
21. Zhao, T. et al. Single-cell RNA-seq reveals dynamic early embryonic-like programs during chemical reprogramming. *Cell Stem Cell* **23**, 31–45 (2018).
22. Li, X. et al. Small-molecule-driven direct reprogramming of mouse fibroblasts into functional neurons. *Cell Stem Cell* **17**, 195–203 (2015).
23. Augsornworawat, P., Maxwell, K. G., Velazco-Cruz, L. & Millman, J. R. Single-cell transcriptome profiling reveals β cell maturation in stem cell-derived islets after transplantation. *Cell Rep.* **32**, 108067 (2020).
24. Zhu, H., Yu, L., He, Y. & Wang, B. Nonhuman primate models of type 1 diabetes mellitus for islet transplantation. *J. Diabetes Res.* **2014**, 785948 (2014).
25. Hecht, G. et al. Embryonic pig pancreatic tissue for the treatment of diabetes in a nonhuman primate model. *Proc. Natl Acad. Sci. USA* **106**, 8659–8664 (2009).
26. Shin, J. S. et al. Long-term control of diabetes in immunosuppressed nonhuman primates (NHP) by the transplantation of adult porcine islets. *Am. J. Transplant.* **15**, 2837–2850 (2015).
27. Tattersall, R. B. Brittle diabetes revisited: the Third Arnold Bloom Memorial lecture. *Diabet. Med.* **14**, 99–110 (1997).
28. Hirsch, I. B. & Gaudiani, L. M. A new look at brittle diabetes. *J. Diabetes Complications* **35**, 107646 (2021).
29. Coe, T. M., Markmann, J. F. & Rickert, C. G. Current status of porcine islet xenotransplantation. *Curr. Opin. Organ Transplant.* **25**, 449–456 (2020).
30. Kim, J. M. & Hong, S. H. Long-term porcine islet graft survival in diabetic non-human primates treated with clinically available immunosuppressants. *Xenotransplantation* **28**, e12659 (2021).
31. Muthyala, S. et al. The effect of hypoxia on free and encapsulated adult porcine islets—an in vitro study. *Xenotransplantation* **24**, 10.1111/xen.12275 (2017).
32. Shin, J. S. et al. Failure of transplantation tolerance induction by autologous regulatory T cells in the pig-to-non-human primate islet xenotransplantation model. *Xenotransplantation* **23**, 300–309 (2016).
33. Graham, M. L., Bellin, M. D., Papas, K. K., Hering, B. J. & Schuurman, H. J. Species incompatibilities in the pig-to-macaque islet xenotransplant model affect transplant outcome: a comparison with allotransplantation. *Xenotransplantation* **18**, 328–342 (2011).
34. Delaune, V., Berney, T., Lacotte, S. & Toso, C. Intraportal islet transplantation: the impact of the liver microenvironment. *Transpl. Int.* **30**, 227–238 (2017).
35. Association, A. D. Standards of medical care in diabetes—2014. *Diabetes Care* **37**, S14–S80 (2014).
36. Sherwani, S. I., Khan, H. A., Ekhzaimy, A., Masood, A. & Sakharkar, M. K. Significance of HbA1c test in diagnosis and prognosis of diabetic patients. *Biomark. Insights* **11**, 95–104 (2016).
37. Ponticelli, C. & Passerini, P. Gastrointestinal complications in renal transplant recipients. *Transpl. Int.* **18**, 643–650 (2005).
38. Peters, A. et al. Posttransplant lymphoproliferative disorder after clinical islet transplantation: report of the first two cases. *Am. J. Transplant.* **17**, 2474–2480 (2017).
39. Sečník, P. Jr. et al. Immunoglobulin abnormalities in 1677 solid organ transplant recipients. Implications for posttransplantation follow-up. *Transpl. Immunol.* **57**, 101229 (2019).
40. Dufrane, D. et al. Streptozotocin-induced diabetes in large animals (pigs/primates): role of GLUT2 transporter and β-cell plasticity. *Transplantation* **81**, 36–45 (2006).
41. Saisho, Y. et al. Ongoing β-cell turnover in adult nonhuman primates is not adaptively increased in streptozotocin-induced diabetes. *Diabetes* **60**, 848–856 (2011).
42. Koulmanda, M. et al. The effect of low versus high dose of streptozotocin in cynomolgus monkeys (*Macaca fascilularis*). *Am. J. Transplant.* **3**, 267–272 (2003).
43. Bottino, R. et al. Recovery of endogenous β-cell function in nonhuman primates after chemical diabetes induction islet. *Transplant. Diabetes* **58**, 442–447 (2009).
44. Zhu, Y., Liu, Q., Zhou, Z. & Ikeda, Y. PDX1, neurogenin-3, and MAFA: critical transcription regulators for beta cell development and regeneration. *Stem Cell Res. Ther.* **8**, 240 (2017).
45. Bastidas-Ponce, A. et al. Foxa2 and Pdx1 cooperatively regulate postnatal maturation of pancreatic β-cells. *Mol. Metab.* **6**, 524–534 (2017).
46. Nordmann, T. M. et al. The role of inflammation in β-cell dedifferentiation. *Sci. Rep.* **7**, 6285 (2017).
47. Eizirik, D. L., Colli, M. L. & Ortis, F. The role of inflammation in insulitis and β-cell loss in type 1 diabetes. *Nat. Rev. Endocrinol.* **5**, 219–226 (2009).
48. Triñanes, J. et al. Deciphering tacrolimus-induced toxicity in pancreatic β cells. *Am. J. Transplant.* **17**, 2829–2840 (2017).
49. Gruessner, R. W. & Gruessner, A. C. What defines success in pancreas and islet transplantation—insulin independence or prevention of hypoglycemia? A review. *Transplant. Proc.* **46**, 1898–1899 (2014).
50. Barton, F. B. et al. Improvement in outcomes of clinical islet transplantation: 1999–2010. *Diabetes Care* **35**, 1436–1445 (2012).
51. Stratton, I. M. et al. Association of glycaemia with macrovascular and microvascular complications of type 2 diabetes (UKPDS 35): prospective observational study. *BMJ* **321**, 405–412 (2000).
52. Warnock, G. L. et al. A multi-year analysis of islet transplantation compared with intensive medical therapy on progression of complications in type 1 diabetes. *Transplantation* **86**, 1762–1766 (2008).
53. Lablanche, S. et al. Islet transplantation versus insulin therapy in patients with type 1 diabetes with severe hypoglycaemia or poorly controlled glycaemia after kidney transplantation (TRIMECO): a multicentre, randomised controlled trial.*Lancet Diabetes Endocrinol.* **6**, 527–537 (2018).
54. Kojayan, G. G., Alexander, M., Imagawa, D. K. & Lakey, J. R. T. Systematic review of islet cryopreservation. *Islets* **10**, 40–49 (2018).
55. Suman, S., Domingues, A., Ratajczak, J. & Ratajczak, M. Z. Potential clinical applications of stem cells in regenerative medicine. *Adv. Exp. Med. Biol.* **1201**, 1–22 (2019).
56. Hentze, H. et al. Teratoma formation by human embryonic stem cells: evaluation of essential parameters for future safety studies. *Stem Cell Res.* **2**, 198–210 (2009).

57. Martin, R. M. et al. Improving the safety of human pluripotent stem cell therapies using genome-edited orthogonal safeguards. *Nat. Commun.* **11**, 2713 (2020).
58. Kimura, Y. et al. Human genomic safe harbors and the suicide gene-based safeguard system for iPSC-based cell therapy. *Stem Cells Transl. Med.* **8**, 627–638 (2019).
59. Wiebking, V., Patterson, J. O. & Martin, R. Metabolic engineering generates a transgene-free safety switch for cell therapy. *Nat. Biotechnol.* **38**, 1441–1450 (2020).
60. Bochenek, M. A. et al. Alginate encapsulation as long-term immune protection of allogeneic pancreatic islet cells transplanted into the omental bursa of macaques. *Nat. Biomed. Eng.* **2**, 810–821 (2018).
61. Ludwig, B. et al. Transplantation of human islets without immunosuppression. *Proc. Natl Acad. Sci. USA* **110**, 19054–19058 (2013).

Methods

Cell sources and culture. Human adipose-derived fibroblasts (hADFs) were isolated from adipose tissues, which were obtained from Shichun Lu (Chinese PLA General Hospital) with informed consent by the donor and approval by the institutional review board (IRB) of Peking University (IRB 00001052-19070). This study was conducted in accordance with the principles of the Declaration of Helsinki. hADFs were cultured in Mesenchymal Stem Cell Growth Medium 2 (PromoCell, C-28009) with supplement mix (PromoCell, C-39809). Medium was changed every 2 d. Primary hADFs were passaged using 0.25% Trypsin-EDTA (Gibco, 25200-056) when confluent, usually every 3–5 d.

Four human chemically induced pluripotent stem cell lines (hCiPSC1, hCiPSC2, hCiPSC3 and hCiPSC4) were induced from hADFs using a chemical reprogramming strategy without gene transfer. The detailed experimental procedures of hCiPSC establishment and thorough characterizations are provided in another manuscript currently under review.

Two induced pluripotent stem cell lines generated by mRNA strategy (hiPSC (mRNA) 1 and hiPSC (mRNA) 2) and one induced pluripotent stem cell line generated using episomal strategy (hiPSC (Episomal) 1) were also induced from hADFs using commercial reprogramming kits (StemRNA 3rd Gen Reprogramming Kit (Stemgent, 00-0076) and Epi Episomal iPSC Reprogramming Kit (Thermo Fisher Scientific, A15960)), according to manufacturer instructions.

Pluripotent stem cell lines were cultured in mTeSR1 (STEMCELL Technologies, 85850) on a 1:40 diluted Matrigel-coated (BD BioSciences, 356231) six-well plate (Corning, 353046) or 500 cm^2 Square TC-treated Culture Dish (Corning, 431110). Medium was changed daily. All cell lines were verified to be mycoplasma-free by using MycoSEQ Mycoplasma Detection Kit (Thermo Fisher Scientific, 4460626). Cultures were passaged by ReleSR (STEMCELL Technologies, 05872) at a 1:10–1:15 split ratio every 5–6 d.

Human islets were gifted by Shusen Wang (Tianjin First Central Hospital) and were cultured in CMRL1066 (Thermo Fisher Scientific, 11530037) containing 10% FBS (Thermo Fisher Scientific, 10099141C) and 1% Pen/Strep (Gibco, 15140-122).

In vitro differentiation to generate hCiPSC-islets. Before differentiation, adherent hCiPSCs (at 80~90% confluence) were dispersed using Accutase (EMD Millipore, SCR005) into single cells, rinsed with DMEM/F12 (Gibco, 11330-032) and seeded at ~1.35×10^5 cells per cm^2 on Matrigel-coated cell factory (Thermo Fisher Scientific, 169171) in mTESR1 supplemented with 10 μM Y27632. Differentiation was initiated 24 h after seeding.

Detailed information of small molecules and cytokines used in the differentiation process is listed in Supplementary Table 7. Medium formulation at each stage is shown as follows:

Stage 1 (4 d). MCDB131 (Gibco, 10372-019) supplemented with 4.5 mM glucose (Sigma-Aldrich, G7021), 1% GlutaMAX (Gibco, 35050-061), 1% Pen/Strep, 1% B27 (Gibco, 12587-010), 100 ng ml^{-1} of activin A, 0.25 mM vitamin C, 6 μM Chir99021, 50 nM PI103 and 10 μM Y27632 for day 1 only. For days 2–4, culture medium was refreshed every day in MCDB131 with 4.5 mM glucose, 1% GlutaMAX, 1% Pen/Strep, 1% B27, 50 ng ml^{-1} of activin A and 0.25 mM vitamin C.

Stage 2 (2 d). MCDB131 supplemented with 4.5 mM glucose, 1% GlutaMAX, 1% Pen/Strep, 0.5% BSA (Sigma-Aldrich, A4612), 50 ng ml^{-1} of KGF, 0.25 mM vitamin C, 5 μM SB431542 and 100 nM Wnt-C59.

Stage 3 (4 d). DMEM-basic (Gibco, C11965500BT) supplemented with 1% B27, 1% Pen/Strep, 2 μM retinoic acid, 0.1 μM LDN193189, 0.25 μM Sant1 and 100 nM Wnt-C59. At the end of Stage 3, the cells were dispersed, incubating with Accutase for 6–8 min at 37 °C. The released cells were rinsed with DMEM-basic and spun down at 300*g* for 3 min. The cells were then seeded at 5×10^6 cells per well in six-well AggreWell Microwell Plates (STEMCELL Technologies, 27940) in Stage 4 medium supplemented with 10 μM Y27632 and spun down to the bottom of the microwells by centrifuging the plates at 300*g* for 5 min. The cells were then incubated in 5% CO_2 at 37 °C for 20 h, and the generated cell clusters were transferred into an ultra-low attachment six-well plate (Beaver Bio, 40406) with Stage 4 medium. Suspended aggregates were cultured in an incubator shaker (INFORS HT, Multitron) at a rotation rate of 90 r.p.m., at 37 °C, 5% CO_2 and 85% humidity.

Stage 4 (5–6 d). DMEM-basic supplemented with 1% GlutaMAX, 1% B27, 1% Pen/Strep, 100 ng ml^{-1} of EGF, 0.2 μM TPB, 10 mM nicotinamide, 0.25 μM Sant1 and 0.25 mM vitamin C.

Stage 5 (6 d). DMEM-basic supplemented with 1% Pen/Strep, 1% GlutaMAX, 1% B27, 10 μM ALK5 inhibitor II, 0.3 μM LDN193189, 1 μM T3, 10 μM ISX9, 10 μg ml^{-1} of heparin, 0.1 μM γ-secretase inhibitor Xxi, 100 nM Wnt-C59, 10 μM Y27632 and 0.25 mM vitamin C. ISX9 was added for 3–6 d starting from Stage 5 Day 1 (S5D1), and the treatment time window was fine-tuned on different cell lines to obtain the optimal β cell differentiation efficiency.

Stage 6 (2–4 d). DMEM-basic supplemented with 1% B27, 1% Pen/Strep, 10 μM ALK5 inhibitor II, 0.5 μM R428, 1 μM T3, 10 μM forskolin, 10 μg ml^{-1} of heparin, 10 μM zinc sulfate, 2 mM *N*-Acetyl-L-cysteine and 0.25 mM vitamin C.

Cryopreservation and recovery of hCiPSC-islets. *Cryopreservation.* hCiPSC-islets were dispersed using Accutase for 12–15 min in the incubator shaker at 90 r.p.m. and 37 °C. Released single cells were rinsed with DMEM-basic and spun down at 300*g* for 3 min. The cells were cryopreserved at a concentration of 1×10^7 cells per ml (1 ml per vial) with a cryopreservation medium consisting of 35% FBS, 5% DMSO (Sigma-Aldrich, D2650) and 60% Stage 6 medium, with 10 μM Y27632. The vials were then transferred into Thermo Fisher Scientific Mr. Frosty (5100–0001) immediately and frozen in a −80 °C freezer for 24 h. Subsequently, the vials were transferred into liquid nitrogen for long-term storage.

Recovery. Cryopreserved vials were thawed in a 37 °C water bath. Cell suspension was then transferred into a 15-ml centrifuge tube containing 10 ml of DMEM-basic medium, followed by centrifugation at 350*g* for 3 min. Cells were resuspended in DMEM-basic supplemented with 1% B27 and 10 μM Y27632. Viability and yield were verified by trypan blue (Invitrogen, T10282) and Countess II Automated Cell Counter (Invitrogen, AMQAX1000). Then, the cells were seeded at 5×10^6 cells per well in six-well AggreWell Microwell Plates and spun down at 300*g* for 5 min into the microwells. After incubating in 5% CO_2 at 37 °C for 20 h, the clusters were transferred into ultra-low attachment six-well plates containing DMEM-basic supplied with 1% B27. Suspended aggregates were cultured in an incubator shaker at a rotation rate of 90 r.p.m. at 37 °C, 5% CO_2 and 85% humidity for 2 d and then were used for transplantation.

Calculation of IEQ of hCiPSC-islets. IEQ of hCiPSC-islets was calculated based on the reported method[62]. The numbers of hCiPSC-islets of certain diameter were counted and recorded using an optical microscope fitted with a reticle (Axio Observer 3, Zeiss). The total IEQ of each batch was determined as (the sum of (number of hCiPSC-islets in diameter class) × (diameter class-specific conversion factor)) × (dilution factor). The number of hCiPSC-islet cells per IEQ (hCiPSC-islet cell number/IEQ) in each batch was then calculated by dividing hCiPSC-islet cell count by IEQ, which was then averaged to obtain the average cell number per IEQ.

Flow cytometry. Cells were released into a single-cell suspension with Accutase and then stained for surface markers and intracellular markers as described previously[17]. Single cells were fixed with Fixation/Permeabilization Solution (BD BioSciences, 554714) for 20 min. Cells were then washed twice in wash buffer (1×) and incubated with primary antibodies overnight at 4 °C. Primary antibodies were diluted with wash buffer (1×). Cells were washed twice in wash buffer (1×) and incubated with secondary antibodies for 1 h at 4 °C. Cells were then washed twice in wash buffer (1×) and analyzed using BD CellQuest Pro. FlowJo version 10 software was used for flow cytometry analysis. The antibodies used are listed in Supplementary Table 8.

Immunohistochemistry and immunofluorescence staining. *For cell cultures.* Cultured cells were washed with PBS and fixed with 4% paraformaldehyde (PFA; Biosharp, BL539A) for 15 min at room temperature. The cells were then washed with PBS and permeabilized with PBST solution (PBS + 0.2% Triton X-100 + 5% donkey serum) for 1 h at room temperature. The samples were then incubated with primary antibodies diluted in PBST solution at 4 °C overnight. After three washes with PBS, the slides were incubated with secondary antibodies conjugated to Alexa Fluor 488, 555 or 647 (Life Technologies) in PBST solution at 1:1,000 for 1 h and stained with DAPI for 5 min at room temperature. Images were captured using a Leica TCS SP8 confocal microscope.

For frozen tissue sections. Cell aggregates or tissue were washed with PBS and fixed with 4% PFA for 2 h (cell aggregates) or 24 h (tissue) at 4 °C. Samples were washed three times with PBS and dehydrated overnight at 4 °C in 30% sucrose solution. The samples were overlaid with OCT (Sakura, 4583) solution and frozen using liquid nitrogen and stored at −80 °C. A freezing microtome was used to cut 10-μm sections, which were placed on slides. The slides were washed with PBS and permeabilized with PBST solution for 1 h at room temperature. The slides were then stained with primary and secondary antibodies as detailed above.

For paraffin sectioning. Samples were fixed using a 10% formalin solution for 7 d at room temperature. These samples were then paraffin embedded and sectioned. Sections were dewaxed in xylene, rehydrated in grades of alcohol (5 min: 100%, 95%, 85% and 70%) and washed in PBS. Hematoxylin and eosin (H&E) staining was performed after rehydration. For immunohistochemistry, slides were submerged in pre-heated antigen retrieval solution and microwaved until boiling for at least 15 min, after which they were left to cool to room temperature. The slides were washed with PBS for 5 min and submerged in blocking reagent for 1 h at room temperature in a humidified, light-protected chamber and then washed with PBS three times. Then, sections were stained with primary and secondary antibodies.

All antibodies used above are listed in Supplementary Table 8.

qRT–PCR. Total RNA was extracted with RNeasy Micro Kit (Qiagen, 74004) following the manufacturer's instructions. Transcript One-Step gDNA Removal and cDNA Synthesis SuperMix (TransGen Biotech, AT311-03) was used to synthesize cDNA. KAPA SYBR FAST Universal qPCR Mix (KAPA Biosystems, KK4601) was used for qRT–PCR analysis, which was performed on a 7500 Real Time PCR system. All relative expression levels were normalized to the housekeeping gene *GAPDH*, and the results were analyzed using the ΔΔCt method. The primers are listed in Supplementary Table 9.

Teratoma assay. hCiPSCs were dispersed by Accutase and collected before injection. Approximately 1×10^6 cells were suspended in 50 µl of Matrigel. The cell mixture was injected subcutaneously into immunodeficient SCID/Beige mice. The animals were euthanized before the tumor size exceeded 1.5 cm in diameter. The teratomas were then embedded in paraffin and processed for H&E staining.

Karyotype analysis. Karyotype (chromosomal G-band) analyses were contracted out to Beijing Jiaen Hospital, using standard protocols for high-resolution G-banding (400G–500G) and analyzed by CytoVision (Leica). For each analysis, at least 20 metaphases were examined. The number of chromosomes, as well as the presence of structural chromosomal abnormalities, was examined.

Glucose-stimulated insulin secretion. Krebs buffer was prepared as follows: 129 mM NaCl, 4.8 mM KCl, 2.5 mM $CaCl_2$, 1.2 mM $MgSO_4$, 1 mM Na_2HPO_4, 1.2 mM KH_2PO_4, 5 mM $NaHCO_3$, 10 mM HEPES and 0.1% BSA dissolved in deionized and sterile filtered water. Krebs buffer (pH 7.3–7.4) containing 2.8 mM glucose, 16.7 mM glucose and 30 mM KCl was prepared and warmed to 37 °C before use.

Static glucose-stimulated insulin secretion. hCiPSC-islets (20–50 clusters) or human islets (20–50 islets) were collected and placed in a 24-well plate and then rinsed twice with Krebs buffer. Cells were incubated successively in Krebs buffer containing 2.8 mM glucose, Krebs buffer containing 16.7 mM glucose and Krebs buffer containing 30 mM KCl at 37 °C for 1 h. Supernatant was collected after each incubation, and cells were rinsed with fresh Krebs buffer at each solution change. Supernatant samples were frozen at −80 °C until detection was conducted. After the assay, cells were dispersed into single cells with Accutase and counted with Countess II Automated Cell Counter.

Dynamic glucose-stimulated insulin secretion. The dynamic function of hCiPSC-islets was assessed with an automated perifusion system (Biorep Perifusion System) as previously reported[19]. hCiPSC-islets were assayed with effluent collected at 100 µl $min^{-1}$and exposed to glucose Krebs buffer and KCl Krebs buffer. A 2.8 mM glucose Krebs buffer was perfused for the first 60 min to equilibration. Then, solutions were switched as follows: 2.8 mM glucose Krebs buffer for 15 min, 16.7 mM glucose Krebs buffer for 30 min, 2.8 mM glucose Krebs buffer for 15 min and 30 mM KCl Krebs buffer for 15 min.

Calcium imaging. Calcium influx dynamics of hCiPSC-islets in response to glucose challenge were assayed as follows. Cluster samples were washed with Krebs buffer and stained with 10 µM Cal-520-AM (AATB) for 45 min at 37 °C and then incubated for 15 min without the dye. Before imaging, hCiPSC-islets were loaded into a chip with microchannel and then immediately staged on a confocal microscope for the acquisition of high-resolution images. Time series images were acquired. Progression of glucose challenges in Krebs buffer during imaging was 2 mM glucose, 20 mM glucose, 2 mM glucose and 30 mM KCl for 10 min, 20 min, 20 min and 10 min, respectively.

ELISA. C-peptide, insulin and glucagon levels were detected using human C-peptide ELISA kit (ALPCO, 80-CPTHU-E10), human insulin ELISA kit (ALPCO, 80-INSHUU-E10) and human glucagon ELISA kit (Mercodia, 10-1271-01) according to manufacturer instructions. ELISA was performed with three technical replicates for all samples except for blood samples from mouse, which were performed with two technical replicates owing to limited samples.

Cryo-electron microscopy. Human islets or hCiPSC-islets were processed as described previously[63] by the Center of Cryo-Electron at Zhejiang University. In brief, human islets or hCiPSC-islets were fixed in 0.1 M phosphate buffer (PB; pH 7.4) containing 4% PFA, 8% glutaraldehyde and 0.2% picric acid at least overnight at 4 °C. After four washes with 0.1 M PB, samples were then post-fixed with 1% OsO_4 and dehydrated, followed by infiltration of acetone and epon resin mixture. Samples were embedded and ultra-thin (70 nm) sectioned before staining with uranyl acetate and lead citrate. Grids were examined with a Tecnai G2 Spirit electron microscope.

Immunogold labeling for transmission electron microscopy. For characterization of secretory granules, immunogold labeling was performed according to the procedures described previously[64,65]. In brief, a fixative containing 4% PFA, 0.1% glutaraldehyde and 4,500 mg L^{-1} of glucose in 200 mM HEPES buffer pH 7.4 was added in equal volume as culture medium to cells in culture at 37 °C. Five minutes later, the fixative solution was removed and replaced by fresh fixative alone for 30 min at room temperature. The cells were then washed with 150 mM glycine solution in PBS twice for 5 min each to quench the free aldehyde. Cells were collected and embedded in 12% gelatin (PanReac AppliChem, 147116.1210) by centrifugation, solidified in ice and cut into 1-mm^3 blocks on a cold plate. The blocks were transferred into 2.3 M sucrose and rotated at 4 °C overnight. Blocks were glued to aluminum specimen holders and frozen in liquid nitrogen. Next, 70-nm cryosections were cut at −120 °C with a diamond immuno knife (cryo immuno 35°, DiATOME) with a cryo-ultramicrotome (Leica Microsystems, FC7) and mounted on 100-mesh formvar/carbon-coated nickel grids. For double immunolabeling, sections were first labeled with rat anti-human C-peptide antibody (DSHB, GN-ID4, 1:60), followed by secondary antibody staining with goat anti-rat IgG (H&L) conjugated to 6-nm colloidal gold (AURION, 806.055, 1:50). Subsequently, the sections were labeled with rabbit anti-human glucagon antibody (Abcam, Ab92517, 1:500), and 15-nm protein A-gold (Cell Microscopy Center, University Medical Center Utrecht, 1:50) was used as the secondary antibody. After labeling, sections were counterstained with 2% methylcellulose and 2% uranyl acetate at a ratio of 9:1. Cryosections were examined at 120 kV under the Tecnai G2 Spirit (Thermo Fisher Scientific) electron microscope equipped with a CCD camera (Orius 832, Gatan).

Transplantation in mouse model. All mouse experimental procedures were performed according to the Animal Protection Guidelines of Peking University. Six-to-eight-week-old male CB17.Cg-Prkdc^{scid}Lyst$^{bg\text{-}J}$/Crl (SCID/Beige) mice were purchased from Beijing Vital River Laboratory Animal Technology Company. The mice were housed on a 12-h light/dark cycle in a temperature-controlled room (22 ± 1 °C) with 40–60% humidity.

Transplantation into STZ-treated diabetic mice. Diabetes was induced by five consecutive days of 16 h fast followed by intraperitoneal (i.p.) injection of 70 mg kg^{-1} of STZ (Selleck, S1312) daily. Approximately 3×10^6 hCiPSC-islets cells were transplanted under the left kidney capsule. Fasting blood glucose levels after 16-h fasting were monitored weekly with a handheld glucometer (Roche, 06870279001) using a tail bleed. Body weights of animals were measured weekly. Glucose-stimulated human C-peptide secretion was assessed by collecting blood samples after 16-h fast and at 30 min after glucose injection (2 g kg^{-1}, 30% solution, i.p.). For glucose tolerance tests, i.p. injection of glucose (2 g kg^{-1}, 30% solution) was performed after 16-h fasting, and blood glucose levels were monitored at the predetermined time points (0 min, 5 min, 15 min, 30 min, 60 min, 90 min and 120 min). Plasma was frozen at −80 °C until human C-peptide analysis.

Transplantation into non-STZ-treated healthy mice. Approximately 3×10^6 hCiPSC-islet cells were transplanted under the left kidney capsule. Blood sample after a 16-h fast was collected biweekly for fasting human C-peptide measurement. Plasma was frozen at −80 °C until human C-peptide analysis.

Single-cell RNA sequencing and analysis. *Single-cell RNA sequencing.* Cells were harvested and resuspended in PBS with 0.04% BSA at 1×10^6 cells per milliliter. Then, cell suspensions were loaded on a Chromium Single Cell Controller (10x Genomics) to generate single-cell gel beads in emulsion (GEMs) by using Chromium Single Cell 5′ Library & Gel Bead Kit version 1 (10x Genomics, 1000006) for monkey PBMCs or Chromium Single Cell 3′ GEM, Library & Gel Bead Kit version 3 (10x Genomics, 1000075) for hCiPSC-islets_S6D2, hCiPSC-islets_10 wpt and human islets. Captured cells were lysed, and the released RNA was barcoded through reverse transcription in individual GEMs. Barcoded cDNAs were pooled and underwent cleanup by using Dynabeads MyOne Silane Beads (Invitrogen, 37002D) and then amplified and underwent cleanup for further next-generation library construction. Single-cell RNA sequencing libraries were prepared using Chromium Single Cell 5′ Library Construction Kit version 1 (10x Genomics, 1000020) for monkey PBMCs or Chromium Single Cell 3′ GEM, Library & Gel Bead Kit version 3 (10x Genomics, 1000075) for hCiPSC-islets_S6D2, hCiPSC-islets_10 wpt and human islets, following instructions provided by the manufacturer. Sequencing was performed on an Illumina HiSeq X Ten with pair-end 150 bp.

Single-cell RNA pre-processing. The sequencing data of hCiPSC-islets_10 wpt were aligned to hg19-and-mm10 genome, whereas sequencing data of hCiPSC-islets_S6D2 and human islets were aligned to hg19 genome, and monkey PBMCs sequencing data were aligned to Mmul_10 genome. We used Cell Ranger (version 3.0.2)[66] to quantify the expression of transcripts in each barcode. The output filtered matrices were loaded into R by the DropletUtils package[67]. For post-transplant sequencing data, we defined barcodes with more than 1,000 hg19 genome-aligned unique molecular identifier (UMI) counts and fewer than 1,000 mm10 genome-aligned UMI counts as human cells. Cell quality control was performed by the R package scater[68]. Low-quality cells were removed from downstream analysis, which include cells with UMI counts of less than median − 3 × MAD (median absolute deviation), or cells with gene count

of less than median − 3 × MAD, or cells with mitochondrial proportion of more than median + 2 × MAD; mitochondrial matrices were not considered in monkey PBMC analysis. The raw UMI counts were then normalized by the scran package[69]. Seurat[70] was used for downstream analysis.

Identification of cell types and differential genes analysis. Variable features were found by the FindVariableFeatures function of Seurat, and principal component analysis (PCA) was performed using RunPCA. Elbow point of scatter plot was applied to decide how many PCs to use. Downstream clustering was performed using the top PCs; FindNeighbors and FindClusters were used to cluster cells; and the RunUMAP function was used for dimensionality reduction. Cell types were identified by canonical markers as reported[19,71]. Monkey cell type identification of monkey PBMCs was based on Azimuth (https://azimuth.hubmapconsortium.org/references/). Differential genes after transplant were identified by the FindMarkers function. Gene Ontology biological process enrichment analysis was conducted by the ClusterProfiler R package[72].

Superimposition with human pancreatic data. We merged S6, transplant and human islet single-cell data together by Seurat (anchors and CCA[70]). Clustering tree was made by the BuildClusterTree function using the top 15 PCs. Maturation score is the average scaled expression (before CCA) of mature genes of individual cell type, as reported[23,73].

Bulk RNA sequencing analysis. We tested quality control using FastQC (version 0.11.8)[74]. The adapter of raw RNA sequencing FASTQ reads were trimmed using TrimGalore (version 0.6.6)[75]. The cleaned RNA sequencing FASTQ reads were aligned to hg19 UCSC human reference genome using STAR (version 2.7.3)[76] with default parameters. Output BAM files were then sorted by SAMtools (version 1.9)[77]. The number of alignments mapped to each gene was counted using htseq-count (version 0.11.3)[78] with parameters '-f bam -r name -s reverse -a 10 -t exon -i gene_id -m union '. The count matrix was variance stabilizing transformed (vst) by vst function in the DEseq2 package[79]. Clustering tree was made on vst matrix using all expressed genes by complete method.

Transplantation in diabetic non-human primate model. All monkey experimental procedures were approved by the Institutional Animal Care and Use Committee of the Institute of Medical Biology, Chinese Academy of Medical Science (ethics no. DWLL201908013). Five male rhesus macaques from the Institute of Medical Biology, Chinese Academy of Medical Science were used as recipients for hCiPCs-islet transplantation.

Diabetes induction. Diabetes was induced according to a previously reported method[24]. In brief, a single dose of STZ (90 mg kg^{-1}, AdooQ, A10868) was injected intravenously (within 5 min) after overnight fasting. STZ was diluted in 0.1 M citrate buffer (pH 4.3–4.5) and immediately administered rapidly intravenously followed by administration of normal saline (40–50 ml) for hydration. Omeprazole (0.5 mg kg^{-1}, Losec, AstraZeneca) was injected to prevent nausea and vomiting after hydration. Blood glucose was monitored every hour over the first 12 h after STZ injection and thereafter four times a day. Exogenous insulin injections commenced 3 d after STZ treatment. The short-acting form of insulin (Humalog, Eli Lilly) and long-acting form of insulin (Lantus, Sanofi-Aventis) were injected subcutaneously. Short-acting insulin was administered according to dosing chart in Supplementary Table 10. The levels of blood glucose, C-peptide and HbA1c were recorded before hCiPSC-islet transplantation.

Immunosuppression strategy. The immunosuppression regimen was started 9 d before transplantation (day 0). The protocol was designed based on previously published studies of porcine islet transplantation in non-human primates, as shown in Supplementary Fig. 6a[25,26].

Induction therapy: rituximab (375 mg m^{-2}, i.v., Rituxan, Roche) was injected on day −9. ATG (5 mg kg^{-1}, i.v., thymoglobuline, Genzyme Polyclonals) was infused on days −5 and −3. Basiliximab (0.3 mg kg^{-1}, Simulect, Novartis) was given on days 0 and 2 after transplantation. Methylprednisolone (10 mg kg^{-1}, i.v., Solu-Medrol, Pfizer), chlorpheniramine maleate tablets (0.1 mg kg^{-1}, p.o., Chengdu First Pharmaceutical Company) and diphenhydramine (0.5 mg kg^{-1}, p.o., Linfen Baozhu Pharmaceutical Company) were administered 10 min before rituximab and ATG treatments to reduce allergic reactions.

Maintenance therapy: belatacept (20 mg kg^{-1}, i.v., Nulojix, Bristol Myers Squibb) was administered on days 0, 4 and 14, after which it was injected biweekly; sirolimus (q.d., p.o., Rapamune, Pfizer) and tacrolimus (b.i.d., p.o., Prograf, Astellas) were administered daily. The dosages of sirolimus and tacrolimus were adjusted according to trough blood levels (tacrolimus 4–10 ng ml^{-1}; sirolimus 4–10 ng ml^{-1}). Blood concentrations of the drugs were tested using Viva-E (Vital Scientific).

Alleviation of instant blood-mediated inflammatory reaction: Cobra Venom Factor (100 U kg^{-1}, i.v., Quidel) was administered on day −1. Etanercept (Enbrel, Pfizer) was used on day 0 (5 mg kg^{-1}, i.v.) and days 3, 7 and 10 (2.5 mg kg^{-1}, i.h.) after transplantation.

Prophylactic and preemptive treatment. To prevent cytomegalovirus infection, ganciclovir (5 mg kg^{-1}, i.v., Luoxin, Shandong Luoxin Pharmaceutical Group Stock Company) was administered from days −5 to −7, followed by valganciclovir (20 mg kg^{-1}, p.o., Valcyte, Roche) daily from day −4 onwards. Aspirin (1.85 mg kg^{-1}, p.o., Yunnan Baiyao Group Company) therapy was used to prevent thrombosis from day 1 after transplantation.

Transplant surgeries. The transplantation procedures were performed as previously reported[26]. After the i.v. administration of propofol (0.5 ml kg^{-1}, Petsun Therapeutics), monkeys were anaesthetized with inhalable isoflurane. Heart rate, temperature, blood oxygenation and blood pressure were monitored in real time during the surgical procedure. To maintain blood glucose levels, 5% glucose was infused. hCiPSC-islets were infused into the portal vein through a jejunal vein after laparotomy. The overall quality of hCiPSC-islet preparations is described in Supplementary Table 3.

To mitigate the instant thrombosis, low-molecular-weight heparin sodium (150 IU kg^{-1}, i.h., Fluxum, Alfasigma) was injected subcutaneously at 2 h and 8 h postoperatively, followed by three times a day for about 1 week. Antibiotic treatment was continued for 7 d. Pain relief medication was administered for 3 d.

Routine tests. C-peptide secretion, body weight, HbA1c, complete blood count, serum creatinine and liver function analysis were routinely performed. The complete blood cell count was done using Sysmex XT-200i. HbA1c, serum creatinine and liver function analysis were assessed using Mindray BS-2000.

Monitoring of peripheral lymphocyte populations. The absolute number of peripheral blood lymphocyte populations was monitored using flow cytometry and complete blood count. In brief, whole blood samples were incubated with specific antibodies for lymphocytes (CD45), T cells (CD3) and B cells (CD20) and then lysed. The data were acquired by BD FACSCalibur.

ABO blood group test. Blood samples were collected from all recipient rhesus macaques and analyzed at Suzhou Xishan Biotechnology for ABO blood group testing.

IVGTT. After an overnight fast, 0.75 g kg^{-1} of 50% glucose was infused i.v. into the monkey within 1 min. Blood glucose concentrations were measured with a handheld glucometer at 0, 5, 15, 30, 60 and 90 min after injection. C-peptide levels at the same time points were measured by ELISA as detailed above.

Arginine stimulation test. C-peptide secretion responses to i.v. arginine were measured at two different plasma glucose levels. In brief, after an overnight fasting, a dose of 70 mg kg^{-1} of 10% arginine hydrochloride (Sigma-Aldrich, A5006) was administered over 30 s, the beginning of which was designated 0 min. Blood samples were collected at 0, 2, 4 and 10 min after the first pulse of arginine. Then, 50% glucose was administered to raise and maintain plasma glucose levels at 20 mM. Fifty minutes after the first pulse of arginine, a second arginine pulse (70 mg kg^{-1}) was given. Blood samples were collected at 0, 2, 4 and 10 min after the second pulse of arginine. C-peptide secretion was measured as previously described.

Autopsy and histological analysis. Full necropsy of all monkeys was performed by an experienced primate pathologist. The tissue specimens of major organs were fixed in 4% PFA and 10% formalin for cryosections and paraffin sections.

Assay for donor-specific antibodies. Donor-specific antibodies (IgG) in the recipient plasma were detected by flow cytometry. Donor hCiPSC-islets were thawed as described above and incubated at single cell with recipient plasma (diluted at 1:50) in 4 °C for 50 min. After three washes with PBS, the cells were incubated with FITC-conjugated anti-monkey IgG antibody at 4 °C for 30 min. Stained cell samples were washed three times before analysis.

ELISpot assay. IFN-γ production was detected using ELISpot Assay Kit (Mabtech, 3421M-2APT-2) according to the manufacturer's instructions. In brief, cryopreserved monkey PBMCs were thawed in RPMI-1640 medium (Gibco, 22400-089) containing 1% GlutaMAX, 1% Pen/Strep and 10% heat-inactivated auto-serum and then seeded at 5×10^5 cells per well on pre-coated IFN-γ plates and co-incubated with hCiPSC-islets at a 1:1 ratio. PBMCs of non-transplanted monkeys or PBMCs alone were used as negative control, whereas PBMCs stimulated with anti-monkey CD3 antibody were used as positive control. After 16-h incubation (37 °C and 5% CO_2), the assay was developed according to the manufacturer's instructions, and the plates were read using an ELISpot reader (AID vSpot Spectrum, VSR078IFL).

Donor-specific antibody-mediated cytotoxicity assay. Donor hCiPSC-islets were thawed and incubated with recipient plasma (diluted at 1:3 and 1:10) at 2×10^5 cells per well in 96-well plates at 37 °C and 5% CO_2 for 30 min (1:3) or 60 min (1:3 or 1:10). Cytotoxicity was measured by Annexin V-FITC/PI Apoptosis Detection Kit (Yeasen, 40302). In brief, after co-incubation, the samples were washed twice

with cold PBS and then stained with 100 µl of 1× binding buffer, 5 µl of Annexin V-FITC and 10 µl of PI Staining Solution for 15 min at room temperature away from light. Then, 400 µl of 1× binding buffer was added to the sample, which was tested by flow cytometry.

Statistics and reproducibility. Data analysis was performed using GraphPad Prism software. Statistical significance was evaluated by *t*-test. Throughout the manuscript, *n* represents number of biological replicates unless otherwise stated. *P* values are presented as follows: $*P<0.05$; $**P<0.005$; $***P<0.0005$; $****P<0.00005$; NS, not significant. For representative images shown in Fig. 1b, Extended Data Figs. 3a and 4a and Supplementary Fig. 1a, similar results were obtained from at least ten biologically independent samples. For representative images shown in Fig. 1c,d, Extended Data Figs. 1e,g, 2d,e, 3b and 4b,e,f and Supplementary Figs. 1b,c,g, 2c and 3g, similar results were obtained from at least three biologically independent samples. Images shown in Extended Data Figs. 5b,d,f,h, 6a,b and 8b–d are representative of ten separate images obtained per sample. Images shown in Extended Data Fig. 7c and 9f are representative of three separate images obtained per sample. Images shown in Figs. 4i and 5f,g, Extended Data Figs. 9c,d, 7a,c, 8e–g, 9e and 10a–c and Supplementary Fig. 7a are representative of five separate images obtained per sample.

Reporting Summary. Further information on research design is available in the Nature Research Reporting Summary linked to this article.

Data availability

The RNA sequencing data reported in this paper have been deposited in the Gene Expression Omnibus under accession number GSE185038. Any other requests for raw or processed data will be reviewed by the Peking University Stem Cell Research Centre to verify whether the data requested are subject to any intellectual property or confidentiality obligations. Data and materials that can be shared will be released via a material transfer agreement. Source data are provided with this paper.

References

62. Lembert, N. et al. Areal density measurement is a convenient method for the determination of porcine islet equivalents without counting and sizing individual islets. *Cell Transplant.* **12**, 33–41 (2003).
63. Zhang, B. et al. A *DNAH17* missense variant causes flagella destabilization and asthenozoospermia. *J. Exp. Med.* **217**, e20182365 (2020).
64. Peters, P. J. & Pierson, J. Immunogold labeling of thawed cryosections. *Methods Cell Biol.* **88**, 131–149 (2008).
65. Slot, J. W. & Geuze, H. J. Cryosectioning and immunolabeling. *Nat. Protoc.* **2**, 2480–2491 (2007).
66. Zheng, G. X. et al. Massively parallel digital transcriptional profiling of single cells. *Nat. Commun.* **8**, 14049 (2017).
67. Lun, A. T. L. et al. EmptyDrops: distinguishing cells from empty droplets in droplet-based single-cell RNA sequencing data. *Genome Biol.* **20**, 63 (2019).
68. McCarthy, D. J., Campbell, K. R., Lun, A. T. & Wills, Q. F. Scater: pre-processing, quality control, normalization and visualization of single-cell RNA-seq data in R. *Bioinformatics* **33**, 1179–1186 (2017).
69. Lun, A. T., McCarthy, D. J. & Marioni, J. C. A step-by-step workflow for low-level analysis of single-cell RNA-seq data with Bioconductor. *F1000Res.* **5**, 2122 (2016).
70. Stuart, T. et al. Comprehensive integration of single-cell data. *Cell* **177**, 1888–1902 (2019).
71. Baron, M. et al. A single-cell transcriptomic map of the human and mouse pancreas reveals inter- and intra-cell population structure. *Cell Syst.* **3**, 346–360 (2016).
72. Yu, G., Wang, L. G., Han, Y. & He, Q. Y. clusterProfiler: an R package for comparing biological themes among gene clusters. *OMICS* **16**, 284–287 (2012).
73. Enge, M. et al. Single-cell analysis of human pancreas reveals transcriptional signatures of aging and somatic mutation patterns. *Cell* **171**, 321–330 (2017).
74. de Sena Brandine, G. & Smith, A. D. Falco: high-speed FastQC emulation for quality control of sequencing data. *F1000Res.* **8**, 1874 (2019).
75. Li, J., Galbo, P. M. Jr. & Gong, W. ZMYND11-MBTD1 induces leukemogenesis through hijacking NuA4/TIP60 acetyltransferase complex and a PWWP-mediated chromatin association mechanism. *Nat. Commun.* **12**, 1045 (2021).
76. Dobin, A. et al. STAR: ultrafast universal RNA-seq aligner. *Bioinformatics* **29**, 15–21 (2013).
77. Li, H. A statistical framework for SNP calling, mutation discovery, association mapping and population genetical parameter estimation from sequencing data. *Bioinformatics* **27**, 2987–2993 (2011).
78. Anders, S., Pyl, P. T. & Huber, W. HTSeq—a Python framework to work with high-throughput sequencing data. *Bioinformatics* **31**, 166–169 (2015).
79. Love, M. I., Huber, W. & Anders, S. Moderated estimation of fold change and dispersion for RNA-seq data with DESeq2. *Genome Biol.* **15**, 550 (2014).

Acknowledgements

This work was supported by the National Key Research and Development Program of China (2017YFA0103000 to H.D., 2018YFA0108102 to H.D. and 2020YFA0803704 to S.W.); the National Natural Science Foundation of China (31521004 to H.D., 31730059 to H.D., 82070805 to S.W., 81870535 to S.W., 82100840 to T.L. and 82100841 to R.L.); the Key Project and Team Program of Tianjin (XB202011 to S.W.); and the CAMS Innovation Fund for Medical Sciences (2021-1-I2M-024 to X.P.). The funders had no role in study design, data collection and analysis, decision to publish or preparation of the manuscript. We thank S. Lu at the Department of Hepatobiliary Surgery, Chinese PLA General Hospital, Beijing, for assistance with providing hADFs; Z. Chen at Shanghai Institute of Biochemistry and Cell Biology for assistance with the dynamic glucose-stimulated insulin secretion assay; Y. Li of the Institute of Medical Biology of CAMS for routine blood and biochemical tests; Q. Yao at the Department of Clinical Pharmacology of First Affiliated Hospital of Kunming Medical University for therapeutic drug monitoring; C. Yang of the Center of Cryo-Electron Microscopy of Zhejiang University for assistance on cryo-electron microscopy; and Y. Hu, Y. Xie and P. Dong at the Core Facilities of School of Life Sciences and the National Center for Protein Sciences at Peking University for their professional technical assistance in electron microscopy sample preparation and image analysis. We thank J. Vaughan at the Salk Institute for Biological Studies and M. Huising at the University of California, Davis for their kind provision of the UCN3 antibody. We thank the following people for their contributions to this study: J. Cao, L. Zou, J. Bai, Y. Yan, F. Bai and L. Xu for clinical assistance with the macaques; Y. Yang and D. Zhang for guidance on immune response experiments; X. Fang, L. Zhao, T. Zhang, J. Ma and H. Liu for technical assistance; X. Zhou for assistance with animal care; C. Wang for guidance on matters of animal research ethics; and B. Liu, W. Lai, J. Xu, Y. Fu, L. Cheng and Y. Lv for discussions in the course of the preparation of this manuscript.

Author contributions

H.D., X.P. and Z.S. supervised the research. H.D. and Y.D. conceived of the experimental design. Z.L., D.S. and S.L. performed most of the non-human primate experiments. S.W. and B.Z. performed cell transplantation surgery in non-human primates. X.W., L.S.Y., Y. L. and G.M. performed the main in vitro experiments. Y.D. and L.S.Y. wrote the manuscript. S.W., Z.L., Y.Z. and Y.W. prepared the cells for transplantation into non-human primates. Y.J. and J.G. performed mice transplantation and conducted related testing. C.L., Y.W., Y.P., S.X. and T.W. performed bulk and single-cell transcriptome sequencing and data analysis. W.Y. and H.L. performed the postmortem anatomical analysis of monkeys and related tests. Z.Z., J.G. and J.W. established the hCiPSC lines. H.R. and C.T. performed the calcium flux assay. J.Z. and Z.C. performed the dynamic glucose-stimulated insulin secretion assay. S.W., R.L., T.L. and L.W. isolated human islets from donor pancreata. S.S. edited and reviewed the manuscript.

Competing interests

The authors declare no competing interests.

Additional information

Extended data is available for this paper at https://doi.org/10.1038/s41591-021-01645-7.

Supplementary information The online version contains supplementary material available at https://doi.org/10.1038/s41591-021-01645-7.

Correspondence and requests for materials should be addressed to Zhongyang Shen, Xiaozhong Peng or Hongkui Deng.

Peer review information *Nature Medicine* thanks Matthias Hebrok and the other, anonymous, reviewer(s) for their contribution to the peer review of this work. Editor recognition statement: Jerome Staal was the primary editor on this article and managed its editorial process and peer review in collaboration with the rest of the editorial team.

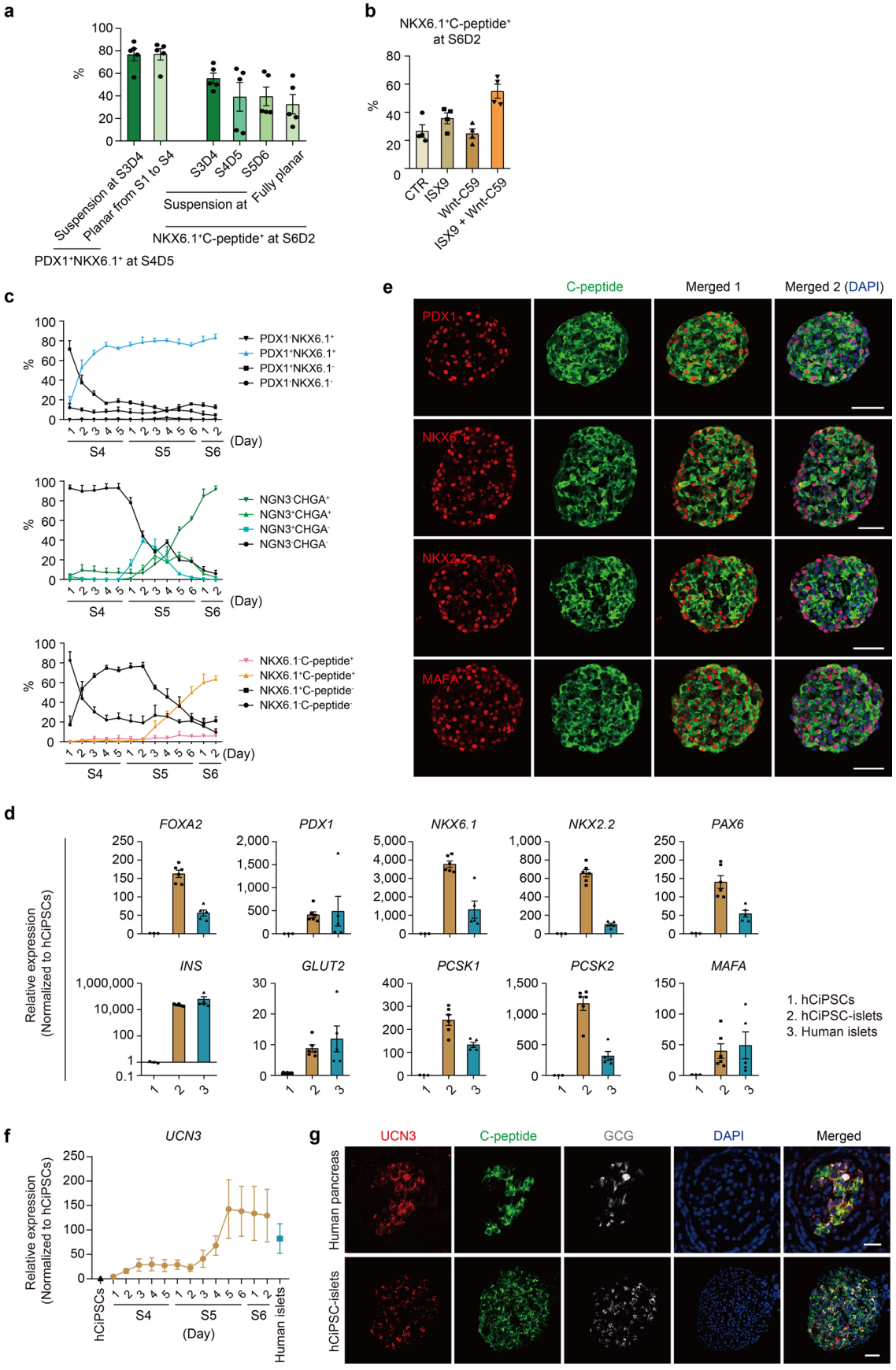

Extended Data Fig. 1 | See next page for caption.

Extended Data Fig. 1 | Establishment of an efficient hCiPSC-islet generation protocol and characterization of hCiPSC-islets. a, Flow cytometry analysis comparing differentiation efficiencies between planar culture and suspension culture at various stages of the protocol in terms of pancreatic progenitor markers at the end of Stage 4 and β cell markers at the end of Stage 6 (n = 5). **b**, Flow cytometry analysis of β cell marker expression in Stage 6 aggregates without and with addition of small molecules ISX9 and Wnt-C59, individually or in combination at Stage 5, detected at S6D2 (n = 4). **c**, Continuous stage-wise tracking of pancreatic progenitor, endocrine progenitor, and β cell markers by flow cytometry throughout the differentiation protocol (n = 3). **d**, qRT-PCR analysis of key pancreatic β cell genes in hCiPSC-islets aggregates (n = 6) and human islets (n = 5). **e**, Representative immunostaining of key β cell transcription factors in sectioned hCiPSC-islets. Scale bar, 50 μm. **f**, Continuous stage-wise tracking of *UCN3* expression by qRT-PCR analysis during hCiPSC-islet differentiation (n = 3) and in human islet sample (n = 3). Relative gene expression was normalized to hCiPSCs (n = 3). **g**, Immunofluorescence staining of UCN3, C-peptide and GCG in sectioned hCiPSC-islet and sectioned human pancreas as control. Scale bar, 25 μm (top), 50 μm (bottom). Similar results were obtained on three independent hCiPSC differentiation batches. Data presented as mean values ± s.e.m.

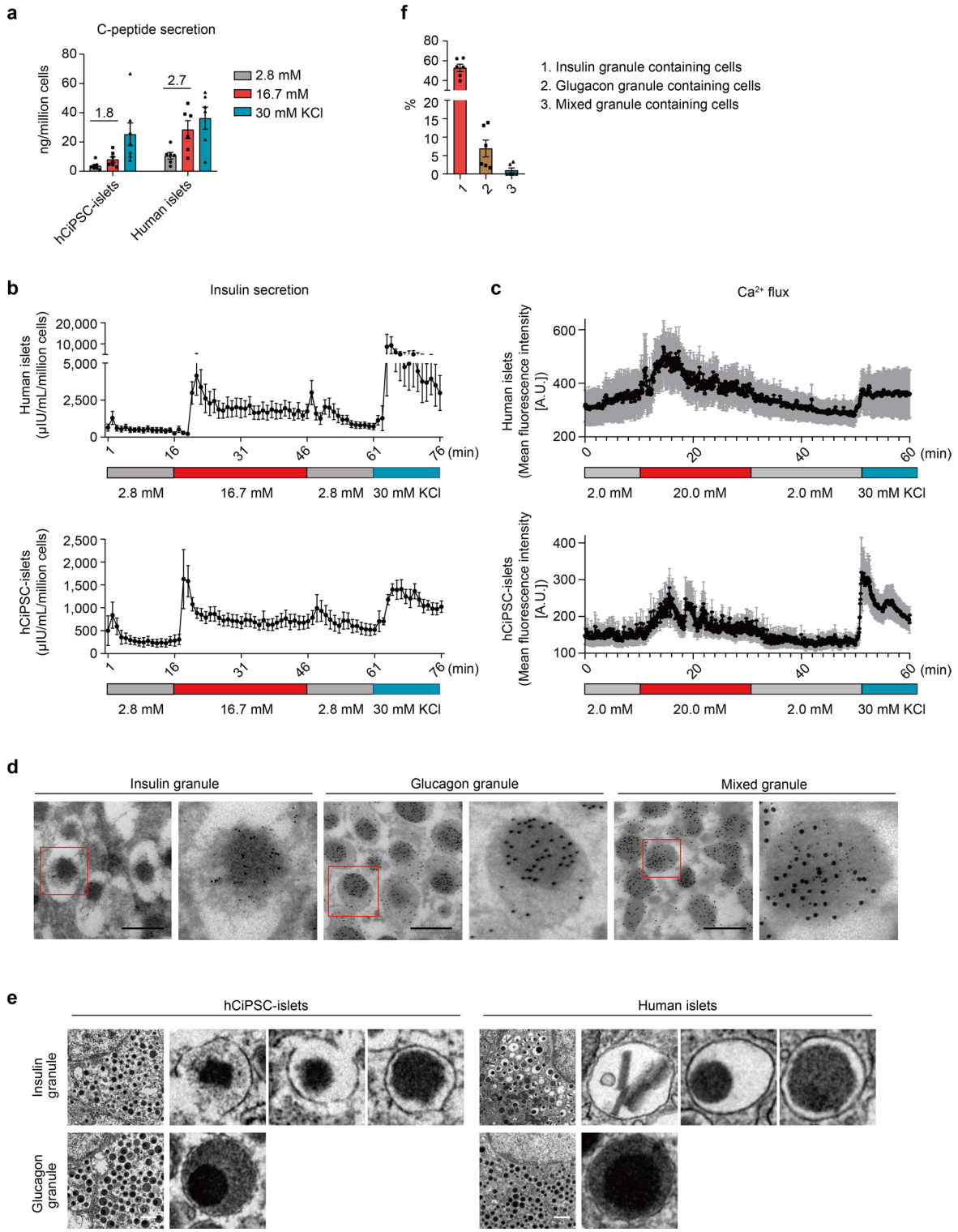

Extended Data Fig. 2 | Characterization of glucose stimulated responses and granule properties of hCiPSC-islets. a, C-peptide secretion of Stage 6 aggregates (n = 7) and primary human islets (n = 6) in static glucose stimulation assay under low glucose (2.8 mM), high glucose (16.7 mM) and depolarization by 30 mM KCl. Glucose stimulation index as indicated above bars. **b**, Insulin secretion of human islets (top; n = 4) and hCiPSC-islets (bottom; n = 5) in dynamic perifusion assay. **c**, Dynamic Cal-520-AM fluorescence intensity trace of human islets (top; n = 10) and hCiPSC-islets (bottom; n = 10) during sequential glucose challenge with low (2 mM), high (20 mM) glucose or depolarization with 30 mM KCl. **d**, Representative immuno-electron micrographs of secretory granules double immunogold labeled with insulin (6 nm) and glucagon (15 nm), with enlarged images of an individual granule shown on the right. Scale bar, 500 nm. **e**, Representative transmission electron micrographs of hCiPSC-islet cells (left) and human islets (right), showing polymorphous crystalline insulin granules (top) or glucagon granules (bottom), with magnified images of representative granules shown on the right. Scale bar, 1 μm. **f**, Proportions of insulin, glucagon and mixed granule containing cells quantified by morphological analysis of TEM images of hCiPSC-islets (n = 6). Data presented as mean values ± s.e.m.

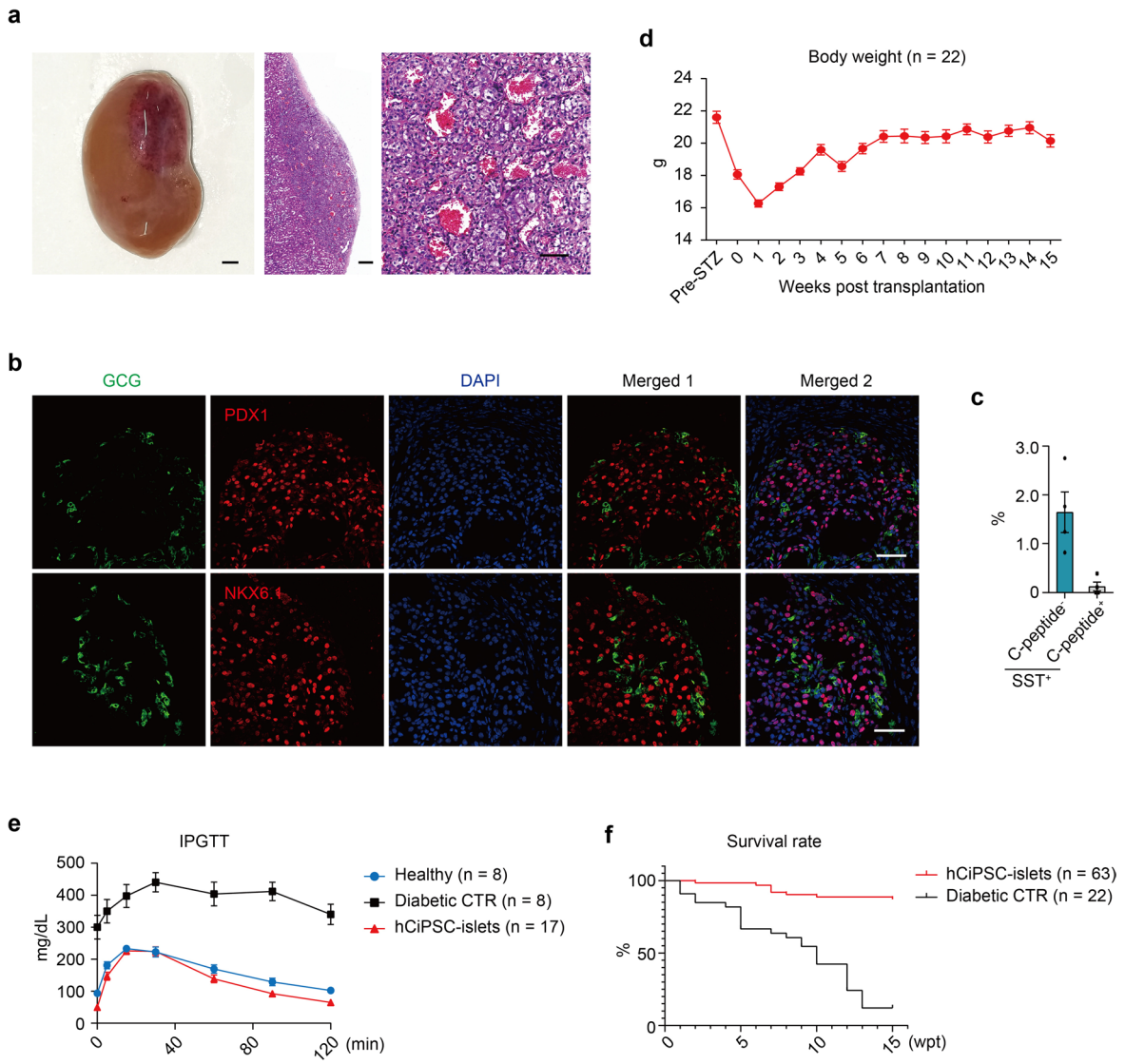

Extended Data Fig. 3 | hCiPSC-islets restored glucose clearance and improved overall survival when transplanted into diabetic mice. a, Left: representative image of nephrectomized kidney showing the hCiPSC-islet graft beneath the kidney capsule. Scale bar, 0.1 cm. Middle, right: H&E histology of kidney section, depicting hCiPSC-islet graft and graft vascularization. Scale bar, 200 μm (middle), 75 μm (right). **b**, Representative immunofluorescence staining of GCG and key β cell transcription factors PDX1 and NKX6.1 in hCiPSC-islet graft sections at 16 wpt. Scale bar, 50 μm. **c**, Quantification of SST and C-peptide expressing subpopulations in hCiPSC-islet graft sections at 16 wpt (n = 4). **d**, Tracking of body weight of hCiPSC-islet transplanted diabetic mice (n = 22). **e**, Changes in blood glucose levels in response to intraperitoneal glucose tolerance test (IPGTT) of healthy (n = 8) and STZ-induced diabetic mice groups with (n = 17) and without (n = 8) hCiPSC-islet transplantation at 16 wpt. **f**, Survival rate of STZ-induced diabetic mice groups with (red; n = 63) and without (black; n = 22) hCiPSC-islet transplantation. Data presented as mean values ± s.e.m.

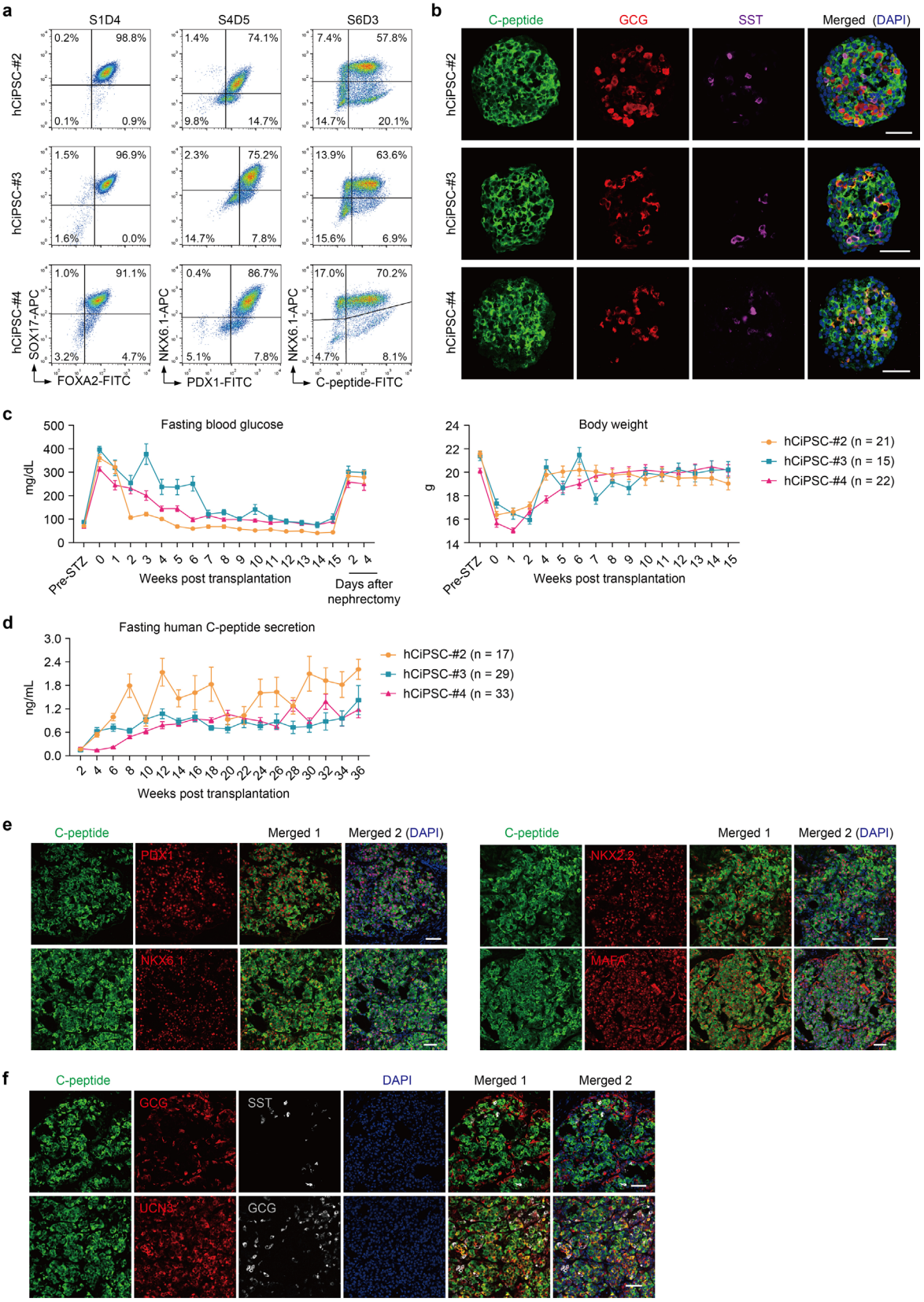

Extended Data Fig. 4 | See next page for caption.

Extended Data Fig. 4 | The established differentiation protocol performed stably across hCiPS cell lines. Similar marker expression pattern and capacity for hyperglycemia reversal were observed across three other hCiPSC lines subject to the established differentiation protocol. **a**, Representative flow cytometry of pancreatic developmental markers during differentiation showed similar distribution and efficiencies along progressive stages across three other hCiPSC lines. **b**, Representative immunofluorescence staining of islet hormones of hCiPSC-islet sections derived from three other independent hCiPSC lines. Scale bar, 50 μm. **c**, Long-term tracking of fasting blood glucose (left) and body weight (right) in diabetic mice transplanted with hCiPSC-islets derived from three other independent hCiPSC lines. **d**, Long-term tracking of fasting human C-peptide secretion in non-diabetic mice. In **c-d**, n = 21, 15 and 22 animals transplanted for hCiPSC line #2, #3 and #4 respectively. **e-f**, Representative immunofluorescence staining of β cell markers (**e**) and islet hormones and maturation marker UCN3 (**f**) in hCiPSC-islet graft at 48 wpt. Scale bar, 50 μm. Data presented as mean values ± s.e.m.

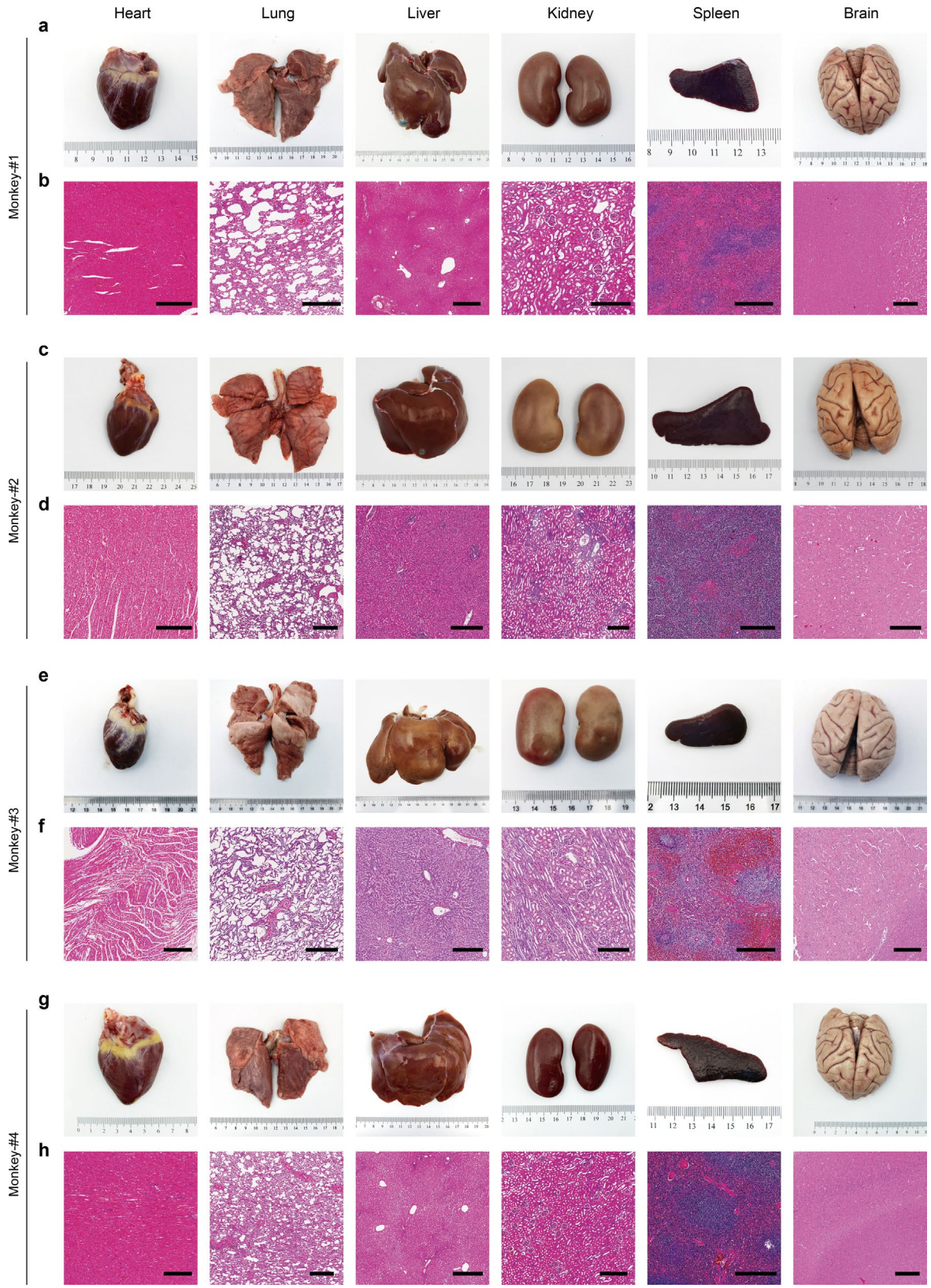

Extended Data Fig. 5 | Postmortem examination of major organs in transplanted diabetic macaques. Gross anatomy (**a, c, e, g**) and H&E staining (**b, d, f, h**) of major organs of Monkey-#1 (**a-b**), Monkey-#2 (**c-d**), Monkey-#3 (**e-f**) and Monkey-#4 (**g-h**). Scale bar, 400 μm.

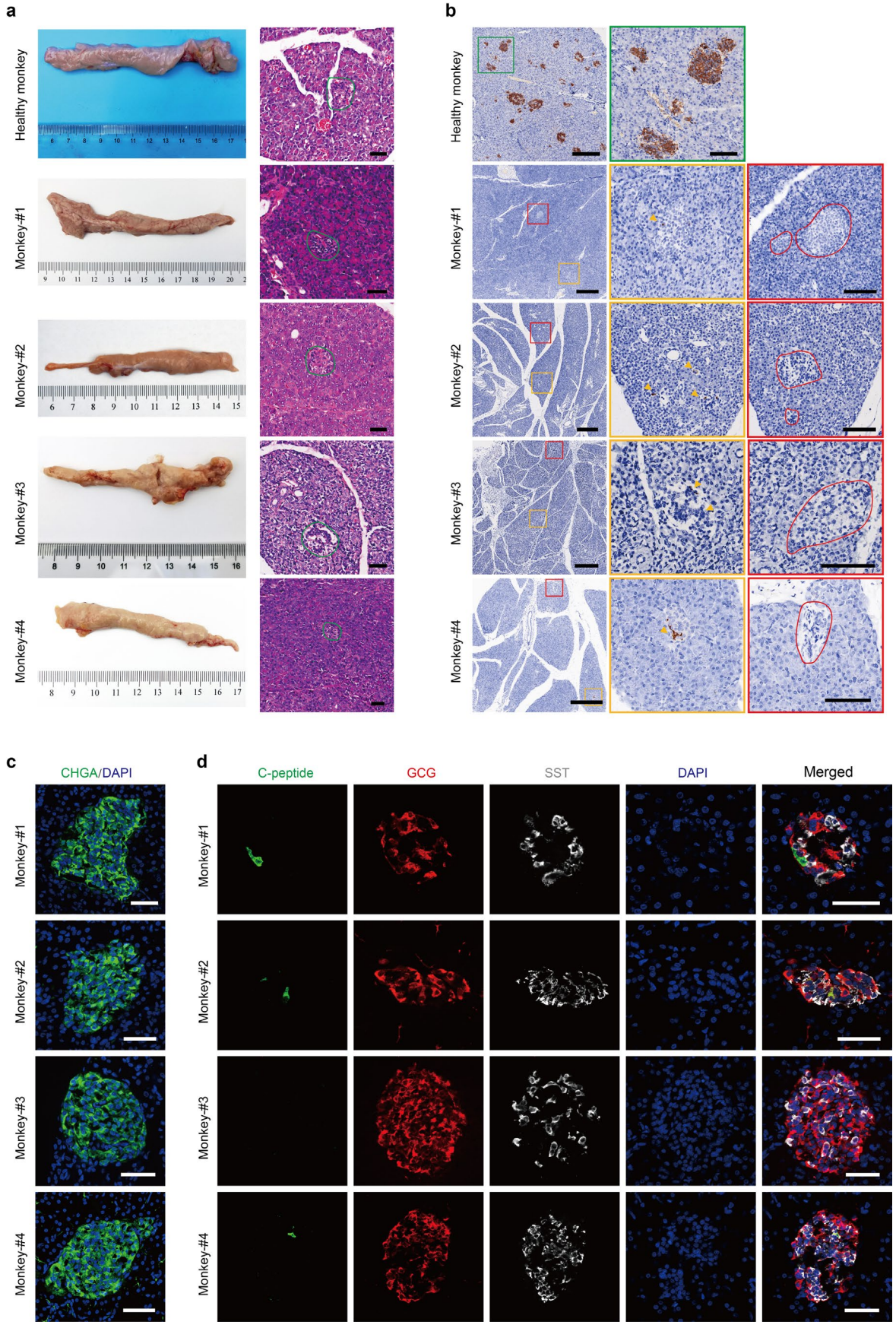

Extended Data Fig. 6 | See next page for caption.

Extended Data Fig. 6 | Gross anatomy, histo- and immunological analysis of native pancreas of STZ-treated recipient monkeys. a, Gross anatomy and H&E staining of pancreas of healthy monkey and recipient Monkey-#1 to #4, with islet structures outlined in green. Scale bar, 50 μm. **b**, Left: C-peptide staining of pancreas sections of healthy control monkey and STZ-treated recipient Monkey-#1 to #4. Scale bar, 400 μm. Middle, Right: Magnified panels of boxed areas. Scale bar, 100 μm. In contrast to pancreas sections of healthy control monkey, pancreas sections of STZ-induced recipient monkeys showed extremely low occurrence of C-peptide positive cells (indicated by yellow arrowheads), with most islets (encircled in red) showing no C-peptide positive cells. **c-d**, Representative immunofluorescence staining of endocrine marker CHGA (**c**) and islets hormone C-peptide, GCG and SST (**d**) in pancreas of STZ-treated recipient Monkey-#1 to #4. Scale bar, 50 μm.

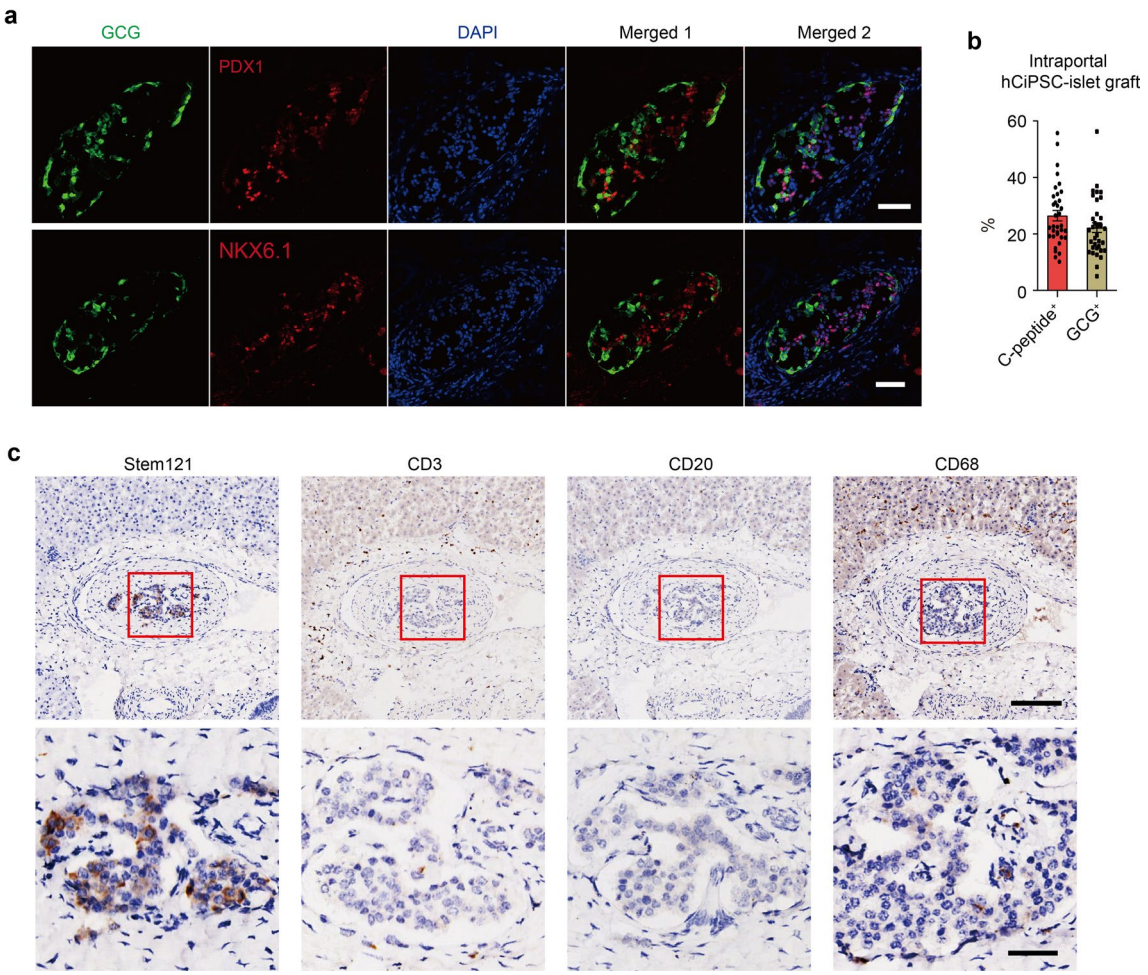

Extended Data Fig. 7 | Immuno- and histological analysis of intrahepatic hCiPSC-islet grafts. a, Representative immunofluorescence staining of GCG and β cell transcription factors PDX1 and NKX6.1 in intrahepatic graft of Monkey-#3 at 101 dpt. Scale bar, 50 μm. **b**, Proportions of C-peptide positive and GCG positive cells in the intraportal-islet grafts in liver sections of Monkey-#3 (n = 35). **c**, Immunohistochemistry staining of human cell-specific marker (Stem121), T cell marker (CD3), B cell marker (CD20) and macrophage marker (CD68) on liver sections of Monkey-#3. Magnified panels shown in bottom row. Scale bar, 200 μm (top), 50 μm (bottom). Data presented as mean values ± s.e.m.

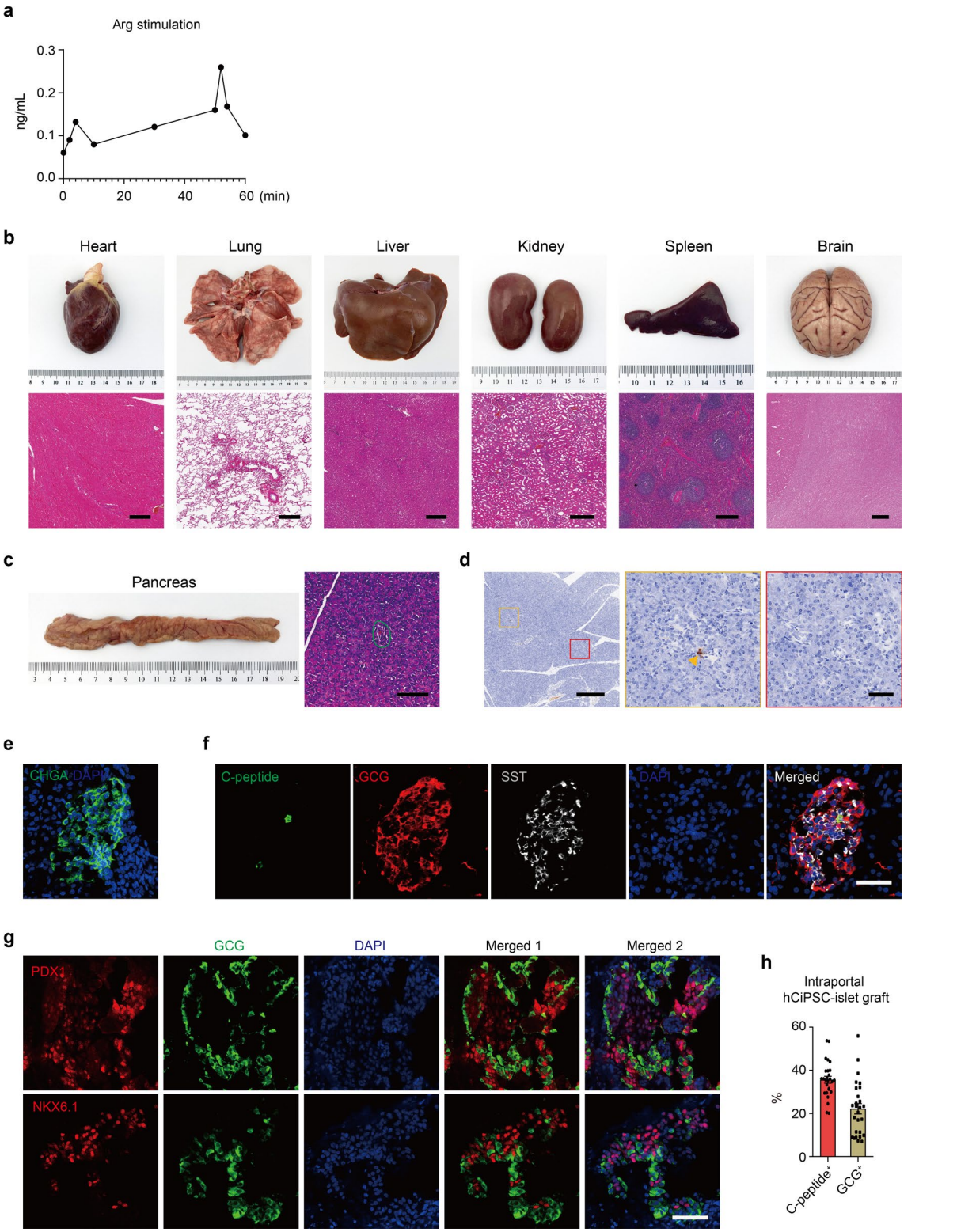

Extended Data Fig. 8 | Metabolic testing and immuno- and histological analysis of Monkey-#5. a, C-peptide secretion in response to glucose potentiated arginine (Arg) stimulation, conducted at 9 wpt (n = 3, technical replicates). **b**, Gross anatomy (top) and H&E staining (bottom) of major organs of Monkey-#5. Scale bar, 400 μm. **c**, Gross anatomy (left) of pancreas and H&E staining of pancreas section (right) of Monkey-#5, with islet structure outlined in green. Scale bar, 100 μm. **d**, Left: C-peptide staining of pancreas sections of STZ-treated recipient Monkey-#5. Scale bar, 400 μm. Middle, Right: magnified panels of boxed areas. C-peptide positive cells are indicated by yellow arrowheads. Scale bar, 50 μm. **e-f**, Representative immunofluorescence staining of endocrine marker CHGA (**e**) and islet hormones (**f**) of pancreatic islets post-STZ treatment in pancreas sections of Monkey-#5. Scale bar, 50 μm. **g**, Representative immunofluorescence staining of GCG and key β cell markers PDX1 and NKX6.1 in intrahepatic hCiPSC-islet grafts in Monkey-#5 liver sections. Scale bar, 50 μm. **h**, Proportions of C-peptide and GCG positive cells in hCiPSC-islet grafts, quantified from immunofluorescence staining of liver sections (n = 27). Data presented as mean values ± s.e.m.

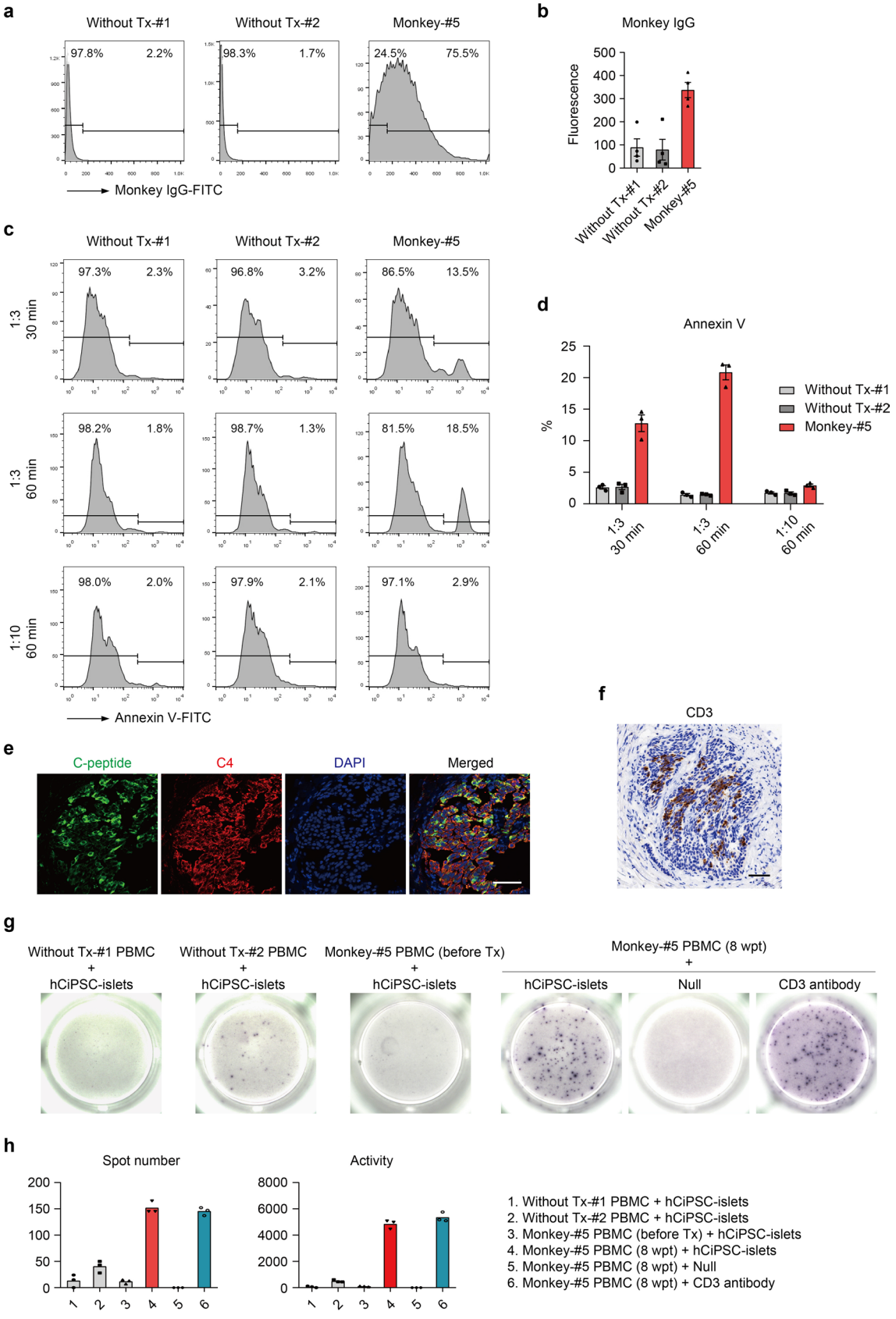

Extended Data Fig. 9 | See next page for caption.

Extended Data Fig. 9 | Immune responses to hCiPSC-islets detected in Monkey-#5. a-b, Flow cytometry histograms (**a**) and peak fluorescence intensities (**b**) depicting fluorescence shift in detection of monkey immunoglobulin G (IgG) in hCiPSC-islet cells co-incubated with serum of recipient Monkey-#5 (sampled at 8 wpt), and serum of two non-transplanted monkeys (Without Tx-#1 and #2) as controls (n = 4). **c-d**, Flow cytometry histograms (**c**) and quantification (**d**) of Annexin V-positive populations in hCiPSC-islet cells co-incubated with serum of recipient Monkey-#5 and serum of two non-transplanted monkeys (Without Tx-#1 and #2) as controls in complement dependent cytotoxicity assay (n = 4). Serum dilutions and incubation periods as indicated on the left. **e**, Immunofluorescence detection of complement (C4) deposition in hepatic hCiPSC-islet grafts in liver sections of Monkey-#5. Scale bar, 50 μm. **f**, Immunohistochemistry staining of CD3 (T cell marker) in hCiPSC-islet containing liver sections of Monkey-#5. Scale bar, 50 μm. **g**, Representative bright field images of IFN-γ ELISpot wells incubated with peripheral blood mononuclear cells (PBMC) of two non-transplanted monkeys (Without Tx-#1 and #2) or Monkey-#5 (sampled pre-transplantation (Pre-Tx) or at 8 wpt), stimulated with hCiPSC-islets. PBMCs of Monkey-#5 post-transplant (8 wpt) alone (Null) or incubated with CD3 antibody were applied as negative and positive control. **h**, Number of spots (left) detected in IFN-γ ELISpot assay and cytokine activity (right) of various incubation conditions as quantified by ELISpot reader analysis (n = 3, technical replicates). Data presented as mean values ± s.e.m.

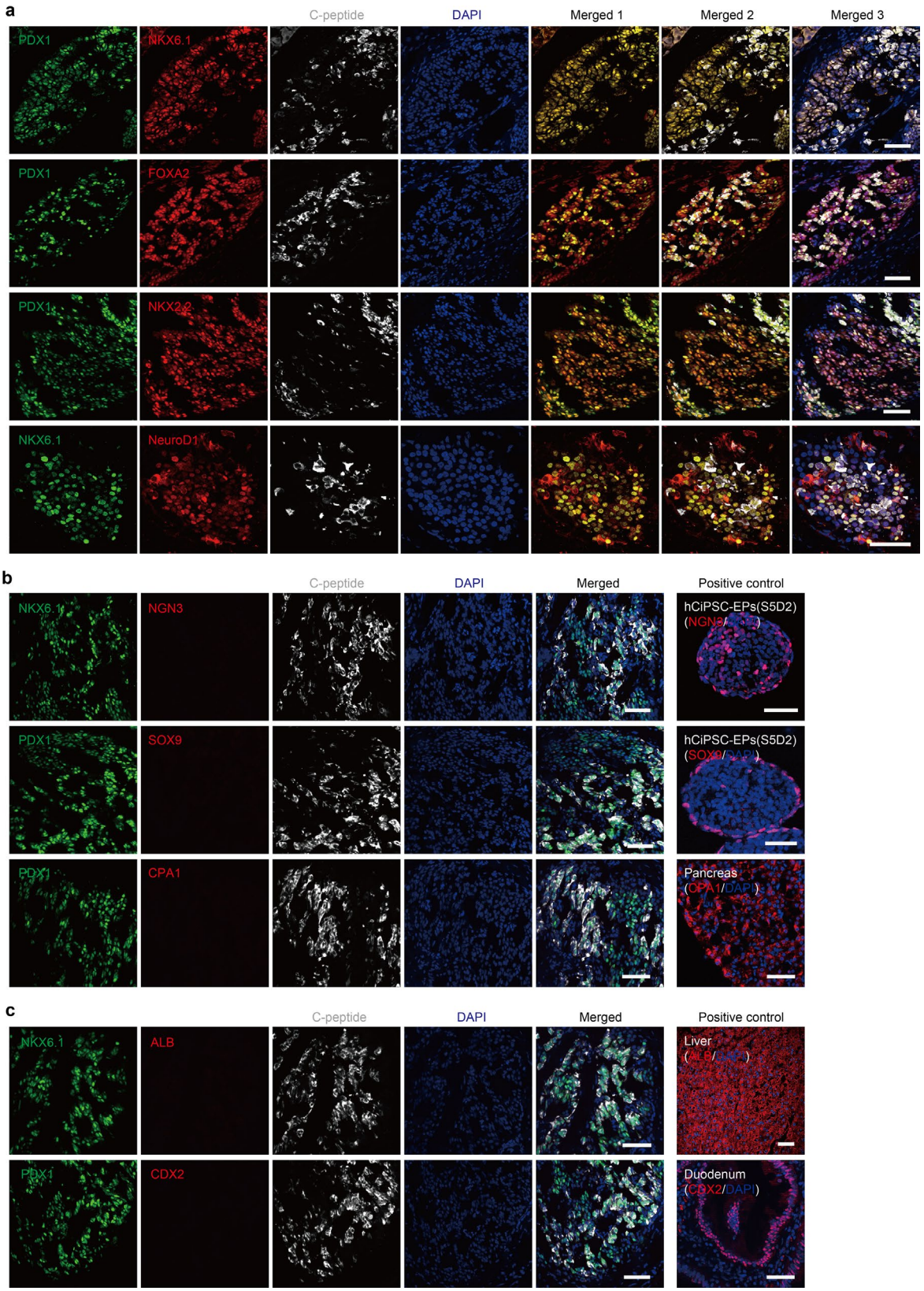

Extended Data Fig. 10 | Characterization of PDX1$^+$NKX6.1$^+$C-peptide$^-$ cells of hepatic hCiPSC-islet grafts by immunofluorescence staining. **a**, PDX1$^+$NKX6.1$^+$C-peptide$^-$ cells were detected in the hepatic hCiPSC-islet grafts at postmortem analysis. They co-express pancreatic endocrine transcription factors (NKX2.2 and NeuroD1) and endodermal transcription factor (FOXA2). **b**, hCiPSC-islet grafts were negative for pancreatic endocrine progenitor marker (NGN3), ductal cell marker (SOX9) or acinar cell marker (CPA1). Corresponding positive staining controls on the right (hCiPSC-derived endocrine progenitors at Stage 5, day 2 or adult pancreas tissue section). **c**, hCiPSC-islet grafts were negative for markers of liver (ALB) and intestine (CDX2) tissue. Corresponding positive staining controls shown on the right (adult liver and duodenal tissue section). Scale bar, 50 μm.

nature research

Corresponding author(s): Hongkui Deng, Zhongyang Shen, Xiaozhong Peng

Last updated by author(s): Nov 11, 2021

Reporting Summary

Nature Research wishes to improve the reproducibility of the work that we publish. This form provides structure for consistency and transparency in reporting. For further information on Nature Research policies, see our Editorial Policies and the Editorial Policy Checklist.

Statistics

For all statistical analyses, confirm that the following items are present in the figure legend, table legend, main text, or Methods section.

n/a	Confirmed
☐	☒ The exact sample size (*n*) for each experimental group/condition, given as a discrete number and unit of measurement
☐	☒ A statement on whether measurements were taken from distinct samples or whether the same sample was measured repeatedly
☐	☒ The statistical test(s) used AND whether they are one- or two-sided *Only common tests should be described solely by name; describe more complex techniques in the Methods section.*
☒	☐ A description of all covariates tested
☒	☐ A description of any assumptions or corrections, such as tests of normality and adjustment for multiple comparisons
☐	☒ A full description of the statistical parameters including central tendency (e.g. means) or other basic estimates (e.g. regression coefficient) AND variation (e.g. standard deviation) or associated estimates of uncertainty (e.g. confidence intervals)
☐	☒ For null hypothesis testing, the test statistic (e.g. *F*, *t*, *r*) with confidence intervals, effect sizes, degrees of freedom and *P* value noted *Give P values as exact values whenever suitable.*
☒	☐ For Bayesian analysis, information on the choice of priors and Markov chain Monte Carlo settings
☒	☐ For hierarchical and complex designs, identification of the appropriate level for tests and full reporting of outcomes
☒	☐ Estimates of effect sizes (e.g. Cohen's *d*, Pearson's *r*), indicating how they were calculated

Our web collection on statistics for biologists contains articles on many of the points above.

Software and code

Policy information about availability of computer code

Data collection

BD FACS Aria IIu flow cytometer was used to run samples, data was acquired by BD CellQuest™ Pro software (Version 6.1).
Immunofluorescence images were captured using Leica TCS SP8 confocal microscope.
qRT-PCR results were acquired using 7500 Real Time PCR Instrument.
The absorbance values for ELISA were acquired by Microplate Spectrophotometer (Thermo Varioskan Lux).
Samples for insulin granules ultrastructure analysis and immunogold labeling were examined with a Tecnai G2 Spirit electron microscope.
The complete blood cell count was done using Sysmex XT-200i.
HbA1c, serum creatinine and liver function analysis were assessed using Mindray BS-2000.
Blood concentrations of the drugs were tested using Viva-E (Vital Scientific N.V.).
Single-cell RNA sequencing was performed on Illumina HiSeq X Ten (Illumina, CA).
ELISpot was read using AID vSpot Spectrum VSR078IFL (GMBH).

Data analysis

Graphpad Prism 8.0.1. was used for statistical analysis.
FlowJo_v10 was used for flow cytometry analysis.
Thermo Scientific SkanIt Software 4.1 was used for ELISA analysis.
Leica Application suite X was used for immunofluorescence image processing.
Cellranger (V3.0.2) (Zheng et al., 2017) to quantify the expression of transcripts in each barcode.
DropletUtils package (Lun et al., 2019) was used for the output filtered matrices.
R package scater (McCarthy et al., 2017) was used to performe cell quality control .
Scran package (Lun et al., 2016) was used to normalize the the raw UMI counts.
Seurat (Stuart et al., 2019) was used for downstream analysis: variable features were found by FindVariableFeatures function of Seurat; principal component analysis (PCA) was performed using the RunPCA; Elbow point of scatter plot was applied to decide how many PCs to use; FindNeighbors and FindClusters were used to cluster cells; RunUMAP function was used for dimensionality reduction; Differential genes after transplant were identified by FindMarkers function; Anchors and CCA was used to merge S6, transplant and human islet single cell data

together; Clustering tree was made by BuildClusterTree function.
GO biological process enrichment analysis was conducted by ClusterProfiler R package (Yu et al., 2012).
The date quality control of Bulk RNA squencing tested using FastQC(V0.11.8) (de Sena Brandine and Smith, 2019).
The adapter of raw RNA sequencing fastq reads were trimmed using TrimGalore (V0.6.6) (Li et al., 2021).
The cleaned RNA sequencing fastq reads were aligned to hg19 UCSC human reference genome using STAR (V2.7.3) (Dobin et al., 2013) with default parameters.
Output bam files were then sorted by samtools (V1.9) (Li, 2011).
The number of alignments mapped to each gene were counted using the htseq-count (V0.11.3) (Anders et al., 2015) with parameters '-f bam -r name -s reverse -a 10 -t exon -i gene_id -m union '.
The count matrix was variance stabilizing transformed (vst) by vst function in DEseq2 package (Love et al., 2014).

For manuscripts utilizing custom algorithms or software that are central to the research but not yet described in published literature, software must be made available to editors and reviewers. We strongly encourage code deposition in a community repository (e.g. GitHub). See the Nature Research guidelines for submitting code & software for further information.

Data

Policy information about availability of data

All manuscripts must include a data availability statement. This statement should provide the following information, where applicable:

- Accession codes, unique identifiers, or web links for publicly available datasets
- A list of figures that have associated raw data
- A description of any restrictions on data availability

The RNA-seq data reported in this paper have been deposited in the Gene Expression Omnibus under accession number GSE185038. Any other requests for raw or processed data will be reviewed by the Peking University Stem Cell Research Centre to verify whether the data requested is subject to any intellectual property or confidentiality obligations. Data and materials that can be shared will be released via a materials transfer agreement.

Field-specific reporting

Please select the one below that is the best fit for your research. If you are not sure, read the appropriate sections before making your selection.

☒ Life sciences ☐ Behavioural & social sciences ☐ Ecological, evolutionary & environmental sciences

For a reference copy of the document with all sections, see nature.com/documents/nr-reporting-summary-flat.pdf

Life sciences study design

All studies must disclose on these points even when the disclosure is negative.

Sample size	Sample sizes were determined based on preliminary experiments and commonly used sample sizes in comparable publications within the field. With in vitro data, sample size used for analysis was 3 - 10. For in vivo data generated using mice, 190 mice were used to evaluate the safety and efficacy of hCiPSC-islets generated from four different hPSC cell lines (hCiPSC-1# n = 53, hCiPSC-2# n = 38, hCiPSC-3# n = 44, hCiPSC-4# n = 55). These sample sizes were sufficient to detect meaningful biological differences with good reproducibility. For in vivo data generated using nonhuman primates, 5 rhesus macaques were used to evaluate the efficacy of hCiPSC-islets. For ethical reasons, a small number of monkeys sufficient to demonstrate good reproducibility was used.
Data exclusions	No data were excluded from the analysis.
Replication	All experiments were conducted with biological replicates of ≥ 3, with the exception of Fig. 4a-d, Fig. 5e and Extended Data 5f, which show technical replicates. All experimental findings were reliably reproduced, and the number of replications were specified in figure legends.
Randomization	The in vitro data were descriptive/observational findings of hCiPSC-islets derived from a differentiation protocol, thus, randomization was not applicable. With transplantation data, animals were allocated into treatment and non-treatment groups randomly.
Blinding	As this was a single-arm study, blinding was not relevant.

Behavioural & social sciences study design

All studies must disclose on these points even when the disclosure is negative.

Study description	*Briefly describe the study type including whether data are quantitative, qualitative, or mixed-methods (e.g. qualitative cross-sectional, quantitative experimental, mixed-methods case study).*
Research sample	*State the research sample (e.g. Harvard university undergraduates, villagers in rural India) and provide relevant demographic information (e.g. age, sex) and indicate whether the sample is representative. Provide a rationale for the study sample chosen. For studies involving existing datasets, please describe the dataset and source.*

Sampling strategy	*Describe the sampling procedure (e.g. random, snowball, stratified, convenience). Describe the statistical methods that were used to predetermine sample size OR if no sample-size calculation was performed, describe how sample sizes were chosen and provide a rationale for why these sample sizes are sufficient. For qualitative data, please indicate whether data saturation was considered, and what criteria were used to decide that no further sampling was needed.*
Data collection	*Provide details about the data collection procedure, including the instruments or devices used to record the data (e.g. pen and paper, computer, eye tracker, video or audio equipment) whether anyone was present besides the participant(s) and the researcher, and whether the researcher was blind to experimental condition and/or the study hypothesis during data collection.*
Timing	*Indicate the start and stop dates of data collection. If there is a gap between collection periods, state the dates for each sample cohort.*
Data exclusions	*If no data were excluded from the analyses, state so OR if data were excluded, provide the exact number of exclusions and the rationale behind them, indicating whether exclusion criteria were pre-established.*
Non-participation	*State how many participants dropped out/declined participation and the reason(s) given OR provide response rate OR state that no participants dropped out/declined participation.*
Randomization	*If participants were not allocated into experimental groups, state so OR describe how participants were allocated to groups, and if allocation was not random, describe how covariates were controlled.*

Ecological, evolutionary & environmental sciences study design

All studies must disclose on these points even when the disclosure is negative.

Study description	*Briefly describe the study. For quantitative data include treatment factors and interactions, design structure (e.g. factorial, nested, hierarchical), nature and number of experimental units and replicates.*
Research sample	*Describe the research sample (e.g. a group of tagged Passer domesticus, all Stenocereus thurberi within Organ Pipe Cactus National Monument), and provide a rationale for the sample choice. When relevant, describe the organism taxa, source, sex, age range and any manipulations. State what population the sample is meant to represent when applicable. For studies involving existing datasets, describe the data and its source.*
Sampling strategy	*Note the sampling procedure. Describe the statistical methods that were used to predetermine sample size OR if no sample-size calculation was performed, describe how sample sizes were chosen and provide a rationale for why these sample sizes are sufficient.*
Data collection	*Describe the data collection procedure, including who recorded the data and how.*
Timing and spatial scale	*Indicate the start and stop dates of data collection, noting the frequency and periodicity of sampling and providing a rationale for these choices. If there is a gap between collection periods, state the dates for each sample cohort. Specify the spatial scale from which the data are taken*
Data exclusions	*If no data were excluded from the analyses, state so OR if data were excluded, describe the exclusions and the rationale behind them, indicating whether exclusion criteria were pre-established.*
Reproducibility	*Describe the measures taken to verify the reproducibility of experimental findings. For each experiment, note whether any attempts to repeat the experiment failed OR state that all attempts to repeat the experiment were successful.*
Randomization	*Describe how samples/organisms/participants were allocated into groups. If allocation was not random, describe how covariates were controlled. If this is not relevant to your study, explain why.*
Blinding	*Describe the extent of blinding used during data acquisition and analysis. If blinding was not possible, describe why OR explain why blinding was not relevant to your study.*

Did the study involve field work? ☐ Yes ☐ No

Field work, collection and transport

Field conditions	*Describe the study conditions for field work, providing relevant parameters (e.g. temperature, rainfall).*
Location	*State the location of the sampling or experiment, providing relevant parameters (e.g. latitude and longitude, elevation, water depth).*
Access & import/export	*Describe the efforts you have made to access habitats and to collect and import/export your samples in a responsible manner and in compliance with local, national and international laws, noting any permits that were obtained (give the name of the issuing authority, the date of issue, and any identifying information).*
Disturbance	*Describe any disturbance caused by the study and how it was minimized.*

Reporting for specific materials, systems and methods

We require information from authors about some types of materials, experimental systems and methods used in many studies. Here, indicate whether each material, system or method listed is relevant to your study. If you are not sure if a list item applies to your research, read the appropriate section before selecting a response.

Materials & experimental systems

n/a	Involved in the study
☐	☒ Antibodies
☐	☒ Eukaryotic cell lines
☒	☐ Palaeontology and archaeology
☐	☒ Animals and other organisms
☒	☐ Human research participants
☒	☐ Clinical data
☒	☐ Dual use research of concern

Methods

n/a	Involved in the study
☒	☐ ChIP-seq
☐	☒ Flow cytometry
☒	☐ MRI-based neuroimaging

Antibodies

Antibodies used

PE anti-human FOXA2, Mouse , BD Biosciences, 561589, 1:200.
APC anti-human SOX17, Mouse, BD Biosciences, 562594, 1:200.
PE anti-human CD3, Mouse, BD Biosciences, 552127, 1:100.
FITC anti-human CD20, Mouse, BD Bioscience,s 556632, 1:100.
APC anti-human CD45, Mouse, BD Biosciences, 561290, 1:100.
PDX1, Goat, R&D, AF2419, 1:200.
PDX1, Rabbit, Abcam, ab219207, 1:200.
NKX6.1, Mouse, DSHB, F55A12-c, 1:200.
NKX6.1, Rabbit, Novus Biologicals, NBP1-49672, 1:200.
NKX6.1, Rabbit, Abcam, ab221549, 1:200.
NKX2.2, Mouse, DSHB, 74.5A5-c, 1:200.
NGN3, Sheep, R&D, AF3444, 1:200.
NeuroD1, Rabbit, Abcam, ab16508, 1:200.
SOX9, Rabbit, Abcam, Ab5535, 1:200.
CDX2, Mouse, BioGenex, MU392A-UC, 1:20.
CPA1, Rabbit, Sigma-Aldrich,HPA021836, 1:200.
ALB, Goat, Bethyl, A80-129A, 1:200.
C-Peptide, Rat, DSHB, GN-ID4, 1:200.
GLUCAGON, Mouse, Sigma-Aldrich, G2654, 1:200.
GLUCAGON, Rabbit, Abcam, Ab92517, 1:500.
MAFA, Rabbit, Novus, NB400-137, 1:200.
UCN3, Rabbit, The Salk Institute for Biological Studies, 1:500.
SOMATOSTATIN, Mouse, Santa Cruz, Sc-55565, 1:200.
CHGA, Rabbit, ZSGB-Bio, ZA-0507, 1:50.
CK19, Mouse, Abcam, Ab7754, 1:1000.
Stem121, Mouse, Cellartis, Y40410, 1:1000.
CD3, Rabbit, Servicebio, GB13014, 1:400.
CD20, Mouse, Servicebio, GB14030, 1:200.
CD68, Mouse, Servicebio, GB14043, 1:400.
OCT4, Rabbit, Invitrogen, MA5-14845, 1:200.
OCT4, Mouse, BD Biosciences, 611203, 1:200.
SOX2, Goat, R&D, AF2018, 1:200.
NANOG, Rabbit, Abcam, ab21624, 1:200.
TRA-1-60, Mouse, Millipore, MAB4360, 1:100.
TRA-1-81, Mouse, Millipore, MAB4381, 1:100.
SSEA-4, Mouse, Santa Cruz, sc-21704, 1:100.
Anti-Rat IgG (6 nm Gold), Goat, Aurion, 806.055, 1:50.
Protein A (15 nm Gold), Rabbit, Cell Microscopy Center, University Medical Center Utrecht, 1:500.
C4, Mouse, Santa Cruz, SC-271181, 1:200.
Anti-Monkey IgG H&L (FITC), Goat, Abcam, ab112766, 1:50.

Validation

PE anti-human FOXA2 (561589) validated by manufacturer for flow cytometry analysis and has been referenced in 4 publications (https://www.citeab.com/antibodies/2407185-561589-bd-pharmingen-pe-mouse-anti-human-foxa2?des=b478801492d73767).
APC anti-human SOX17 (562594) validated by manufacturer for flow cytometry analysis and has been referenced in 5 publications (https://www.citeab.com/antibodies/2407306-562594-bd-pharmingen-alexa-fluor-647-mouse-anti-hu?des=325875b0e3fcefb0).
PE anti-human CD3 (552127) validated by manufacturer for flow cytometry analysis and has been referenced in 19 publications (https://www.citeab.com/antibodies/2409938-552127-bd-pharmingen-pe-mouse-anti-human-cd3?des=c0d6e738aea00c3b).
FITC anti-human CD20 (556632) validated by manufacturer for flow cytometry analysis and has been referenced in 7 publications (https://www.citeab.com/antibodies/2410865-556632-bd-pharmingen-fitc-mouse-anti-human-cd20?des=70b5a78ded732381).
APC anti-human CD45 (561290) validated by manufacturer for flow cytometry analysis and has been referenced in 4 publications (https://www.citeab.com/antibodies/2408819-561290-bd-pharmingen-apc-mouse-anti-nhp-cd45?des=1147abf32ac4647a).

PDX1 (AF2419) validated by manufacturer for IF staining and has been used for IF staining or flow cytometry analysis in 68 publications (https://www.citeab.com/antibodies/688939-af2419-human-pdx-1-ipf1-antibody?des=fc310193d7b2bec2).
PDX1 (ab219207) validated by manufacturer for IF staining and has been referenced in 1 publications (https://www.citeab.com/antibodies/6149301-ab219207-anti-pdx1-antibody-epr22002?des=dacfaa3105dcd24d).
NKX6.1 (F55A12-c) validated by manufacturer for IF staining and flow cytometry analysis and has been referenced in 47 publications (https://www.citeab.com/antibodies/149953-f55a12-homeobox-protein-nkx-6-1-nkx6-1?des=6d19d4d1892e90de).
NKX6.1 (NBP1-49672) validated by manufacturer for IF staining and has been referenced in 7 publications (https://www.citeab.com/antibodies/466846-nbp1-49672-nkx6-1-antibody?des=3cfd035504c141b0).
NKX6.1 (ab221549) validated by manufacturer for IF staining and has been referenced in 5 publications (https://www.citeab.com/antibodies/4637200-ab221549-anti-nkx6-1-antibody-epr20405?des=e0315b665b2232b7).
NKX2.2 (74.5A5-c) validated by manufacturer for IF staining and flow cytometry analysis and has been referenced in 193 publications (https://www.citeab.com/antibodies/150827-74-5a5-nkx2-2-transcription-factor?des=731851838cf547e7).
NGN3 (AF3444) validated by manufacturer for IH staining and has been referenced in 17 publications (https://www.citeab.com/antibodies/690152-af3444-human-neurogenin-3-antibody?des=b60f2685395e384e).
NeuroD1 (ab16508) validated by manufacturer for IF staining and has been referenced in 13 publications (https://www.citeab.com/antibodies/778995-ab16508-anti-neurod1-antibody?des=6eeadedfc8a19a93).
SOX9 (Ab5535) validated by manufacturer for IF staining and has been referenced in 738 publications (https://www.citeab.com/antibodies/223650-ab5535-anti-sox9-antibody?des=0dfdfb9e3fb7ae18).
CDX2 (MU392A-UC) validated by manufacturer for IH staining.
CPA1 (HPA021836) validated by manufacturer for IH staining and has been referenced in 2 publications (https://www.sigmaaldrich.cn/CN/zh/product/sigma/hpa021836?context=product).
ALB (A80-129A) validated by manufacturer for IF staining and has been referenced in 45 publications (https://www.citeab.com/antibodies/2870998-a80-129a-human-albumin-antibody?des=600c984e6629075c).
C-Peptide (GN-ID4) validated by manufacturer for IF staining and flow cytometry analysis and has been referenced in 41 publications (https://www.citeab.com/antibodies/150572-gn-id4-insulin-proinsulin-c-peptide?des=73101e88c818ffed).
GLUCAGON (G2654) validated by manufacturer for IF staining and flow cytometry analysis and has been referenced in 237 publications (https://www.citeab.com/antibodies/2303806-g2654-monoclonal-anti-glucagon-antibody-produced-in?des=579a8db0b9e9e50c).
GLUCAGON (Ab92517) validated by manufacturer for IH staining and has been referenced in 47 publications (https://www.citeab.com/antibodies/733349-ab92517-anti-glucagon-antibody-ep3070?des=57478895b2feca6d).
MAFA (NB400-137) validated by manufacturer for IF staining and has been referenced in 40 publications (https://www.citeab.com/antibodies/408148-nb400-137-mafa-antibody?des=b0af8e23d547d021).
UCN3, The Salk Institute for Biological Studies. This antibody is produced by Dr. Huising at UC Davis and this antibody used for IF staining in at least two cited studies (van der Meulen T et al., PLoS One, 2012;7(12):e52181., van der Meulen T et al., Nature Medicine, 2015, 21(7):769-76.).
SOMATOSTATIN (Sc-55565) validated by manufacturer for IF staining and has been referenced in 16 publications (https://www.citeab.com/antibodies/836427-sc-55565-anti-somatostatin-antibody-g-10?des=2fa36dc36f5c3635).
CHGA (ZA-0507) validated by manufacturer for IF staining.
CK19 (Ab7754) validated by manufacturer for IF staining and has been referenced in 43 publications (https://www.citeab.com/antibodies/726284-ab7754-anti-cytokeratin-19-antibody-a53-b-a2-cyto?des=e33b64cf93c02385).
Stem121 (Y40410) validated by manufacturer for IF staining and has been used for IF staining in 1 publications (Ratnesh K Singh et al., Stem Cells Dev, 2019, ;28(17):1151-1166.).
CD3 (GB13014) validated by manufacturer for IH staining and has been referenced in 8 publications (https://www.citeab.com/antibodies/10504478-gb13014-anti-cd3-rabbit-mab?des=ee3ef42ece1fc01e).
CD20 (GB14030) validated by manufacturer for IH staining.
CD68 (GB14043) validated by manufacturer for IH staining and has been referenced in 2 publications (https://www.citeab.com/antibodies/10504732-gb14043-anti-cd68-mouse-mab?des=8afc6c34dd05ddc0).
OCT4 (MA5-14845) validated by manufacturer for IF staining and flow cytometry analysis and has been referenced in 4 publications (https://www.citeab.com/antibodies/90348-ma5-14845-oct4-monoclonal-antibody-t-631-9?des=f5fea0f4dfcf6a95).
OCT4 (611203) validated by manufacturer for IF staining and has been referenced in 53 publications (https://www.citeab.com/antibodies/2412015-611203-bd-transduction-laboratories-purified-mouse?des=b5d6a9496cf433ac).
SOX2 (AF2018) validated by manufacturer for IF staining and has been referenced in 252 publications (https://www.citeab.com/antibodies/690455-af2018-human-mouse-rat-sox2-antibody?des=bb28e831f1f844d8).
NANOG (ab21624) validated by manufacturer for IF staining and has been referenced in 229 publications (https://www.citeab.com/antibodies/768634-ab21624-anti-nanog-antibody?des=ba5282065528fac6).
TRA-1-60 (MAB4360) validated by manufacturer for IF staining and has been referenced in 360 publications (https://www.citeab.com/antibodies/226508-mab4360-anti-tra-1-60-antibody-clone-tra-1-60?des=5c569352260fcc34).
TRA-1-81 (MAB4381) validated by manufacturer for IF staining.
SSEA-4 (sc-21704) validated by manufacturer for IF staining and has been referenced in 267 publications (https://www.citeab.com/antibodies/226520-mab4381-anti-tra-1-81-antibody-clone-tra-1-81?des=07cc32651a9e25b5).
Anti-Rat IgG (6 nm Gold) (806.055.) validated by manufacturer for immunogold labeling.
Protein A (15 nm Gold) validated by manufacturer for immunogold labeling.
C4 (SC-271181) validated by manufacturer for IF staining and has been referenced in 5 publications (https://datasheets.scbt.com/sc-271181.pdf).
Anti-Monkey IgG H&L (FITC) (ab112766) validated by manufacturer for flow cytometry analysis and has been referenced in 1 publications (https://journals.asm.org/doi/10.1128/mBio.02994-19)

Eukaryotic cell lines

Policy information about cell lines

Cell line source(s)	The four human chemically induced pluripotent stem cell lines (hCiPSC-1#, hCiPSC-2#, hCiPSC-3#, hCiPSC-4#) were generated from human somatic cells using a chemical approach. Human induced pluripotent stem cell lines (hiPSC (mRNA) - #1, hiPSC (mRNA) - #2 and hiPSC (Episomal) - #1) were generated using reported mRNA or episomal reprogramming methods.

Authentication	Human pluripotent stem cell lines were validated by morphology check, pluripotency biomarker analysis, developmental potency, growth curve analysis, identity verification with STR analysis and mycoplasma detection.
Mycoplasma contamination	All cell lines were verified to be mycoplasma-free by using MycoSEQ™ Mycoplasma Detection Kit (Thermo Scientific, Cat# 4460626).
Commonly misidentified lines (See ICLAC register)	No commonly misidentified cell lines were used in this study.

Palaeontology and Archaeology

Specimen provenance	*Provide provenance information for specimens and describe permits that were obtained for the work (including the name of the issuing authority, the date of issue, and any identifying information).*
Specimen deposition	*Indicate where the specimens have been deposited to permit free access by other researchers.*
Dating methods	*If new dates are provided, describe how they were obtained (e.g. collection, storage, sample pretreatment and measurement), where they were obtained (i.e. lab name), the calibration program and the protocol for quality assurance OR state that no new dates are provided.*

☐ Tick this box to confirm that the raw and calibrated dates are available in the paper or in Supplementary Information.

Ethics oversight	*Identify the organization(s) that approved or provided guidance on the study protocol, OR state that no ethical approval or guidance was required and explain why not.*

Note that full information on the approval of the study protocol must also be provided in the manuscript.

Animals and other organisms

Policy information about studies involving animals; ARRIVE guidelines recommended for reporting animal research

Laboratory animals	Mouse experiments were conducted on six to eight week-old CB17.Cg-PrkdcscidLystbg-J/Crl (Scid/Beige) male mice. Nonhuman primate experiments were conducted on 4-6 year-old male rhesus macaques.
Wild animals	This study did not involve wild animals.
Field-collected samples	This study did not involve samples collected from the field.
Ethics oversight	All mouse experimental procedures were performed according to the Animal Protection Guidelines of Peking University, China. All monkey experimental procedures were approved by the Institutional Animal Care and Use Committee of Institute of Medical Biology, Chinese Academy of Medical Science (Ethics number: DWLL201908013).

Note that full information on the approval of the study protocol must also be provided in the manuscript.

Human research participants

Policy information about studies involving human research participants

Population characteristics	*Describe the covariate-relevant population characteristics of the human research participants (e.g. age, gender, genotypic information, past and current diagnosis and treatment categories). If you filled out the behavioural & social sciences study design questions and have nothing to add here, write "See above."*
Recruitment	*Describe how participants were recruited. Outline any potential self-selection bias or other biases that may be present and how these are likely to impact results.*
Ethics oversight	*Identify the organization(s) that approved the study protocol.*

Note that full information on the approval of the study protocol must also be provided in the manuscript.

Clinical data

Policy information about clinical studies

All manuscripts should comply with the ICMJE guidelines for publication of clinical research and a completed CONSORT checklist must be included with all submissions.

Clinical trial registration	*Provide the trial registration number from ClinicalTrials.gov or an equivalent agency.*
Study protocol	*Note where the full trial protocol can be accessed OR if not available, explain why.*
Data collection	*Describe the settings and locales of data collection, noting the time periods of recruitment and data collection.*
Outcomes	*Describe how you pre-defined primary and secondary outcome measures and how you assessed these measures.*

Dual use research of concern

Policy information about dual use research of concern

Hazards

Could the accidental, deliberate or reckless misuse of agents or technologies generated in the work, or the application of information presented in the manuscript, pose a threat to:

No	Yes	
☐	☐	Public health
☐	☐	National security
☐	☐	Crops and/or livestock
☐	☐	Ecosystems
☐	☐	Any other significant area

Experiments of concern

Does the work involve any of these experiments of concern:

No	Yes	
☐	☐	Demonstrate how to render a vaccine ineffective
☐	☐	Confer resistance to therapeutically useful antibiotics or antiviral agents
☐	☐	Enhance the virulence of a pathogen or render a nonpathogen virulent
☐	☐	Increase transmissibility of a pathogen
☐	☐	Alter the host range of a pathogen
☐	☐	Enable evasion of diagnostic/detection modalities
☐	☐	Enable the weaponization of a biological agent or toxin
☐	☐	Any other potentially harmful combination of experiments and agents

ChIP-seq

Data deposition

☐ Confirm that both raw and final processed data have been deposited in a public database such as GEO.

☐ Confirm that you have deposited or provided access to graph files (e.g. BED files) for the called peaks.

Data access links *May remain private before publication.*	*For "Initial submission" or "Revised version" documents, provide reviewer access links. For your "Final submission" document, provide a link to the deposited data.*
Files in database submission	*Provide a list of all files available in the database submission.*
Genome browser session (e.g. UCSC)	*Provide a link to an anonymized genome browser session for "Initial submission" and "Revised version" documents only, to enable peer review. Write "no longer applicable" for "Final submission" documents.*

Methodology

Replicates	*Describe the experimental replicates, specifying number, type and replicate agreement.*
Sequencing depth	*Describe the sequencing depth for each experiment, providing the total number of reads, uniquely mapped reads, length of reads and whether they were paired- or single-end.*
Antibodies	*Describe the antibodies used for the ChIP-seq experiments; as applicable, provide supplier name, catalog number, clone name, and lot number.*
Peak calling parameters	*Specify the command line program and parameters used for read mapping and peak calling, including the ChIP, control and index files used.*
Data quality	*Describe the methods used to ensure data quality in full detail, including how many peaks are at FDR 5% and above 5-fold enrichment.*
Software	*Describe the software used to collect and analyze the ChIP-seq data. For custom code that has been deposited into a community repository, provide accession details.*

Flow Cytometry

Plots

Confirm that:

☒ The axis labels state the marker and fluorochrome used (e.g. CD4-FITC).

☒ The axis scales are clearly visible. Include numbers along axes only for bottom left plot of group (a 'group' is an analysis of identical markers).

☒ All plots are contour plots with outliers or pseudocolor plots.

☒ A numerical value for number of cells or percentage (with statistics) is provided.

Methodology

Sample preparation	Approximately 10^6 cells were dispersed into single cells using Accutase, fixed and permeabilized using BD Cytofix/Cytoperm Buffer (BD Biosciences) at 4°C for 20 mins, followed by three washes in BD Perm/Wash Buffer. Fixed cells were incubated in primary antibody buffer at 4°C overnight. Cells were then washed twice and incubated with secondary antibody for at 4°C for 1 hour. Stained cells were washed twice in Perm/Wash Buffer prior to analysis. All antibodies used and their dilutions can be found in Supplementary Table 2.
Instrument	BD FACS Aria IIu flow cytometer
Software	Data was acquired by BD CellQuest™ Pro.(FlowJo_v10 was used for flow cytometry analysis.
Cell population abundance	No cell sorting was conducted in this study.
Gating strategy	Flow cytometry data was first gated according to scatter properties and viability, then subsequently gated based on clustering of subpopulations to distinguish between negative, single-positive and double-positive subpopulations.

☒ Tick this box to confirm that a figure exemplifying the gating strategy is provided in the Supplementary Information.

Magnetic resonance imaging

Experimental design

Design type	*Indicate task or resting state; event-related or block design.*
Design specifications	*Specify the number of blocks, trials or experimental units per session and/or subject, and specify the length of each trial or block (if trials are blocked) and interval between trials.*
Behavioral performance measures	*State number and/or type of variables recorded (e.g. correct button press, response time) and what statistics were used to establish that the subjects were performing the task as expected (e.g. mean, range, and/or standard deviation across subjects).*

Acquisition

Imaging type(s)	*Specify: functional, structural, diffusion, perfusion.*
Field strength	*Specify in Tesla*
Sequence & imaging parameters	*Specify the pulse sequence type (gradient echo, spin echo, etc.), imaging type (EPI, spiral, etc.), field of view, matrix size, slice thickness, orientation and TE/TR/flip angle.*
Area of acquisition	*State whether a whole brain scan was used OR define the area of acquisition, describing how the region was determined.*

Diffusion MRI ☐ Used ☐ Not used

Preprocessing

Preprocessing software	*Provide detail on software version and revision number and on specific parameters (model/functions, brain extraction, segmentation, smoothing kernel size, etc.).*
Normalization	*If data were normalized/standardized, describe the approach(es): specify linear or non-linear and define image types used for transformation OR indicate that data were not normalized and explain rationale for lack of normalization.*
Normalization template	*Describe the template used for normalization/transformation, specifying subject space or group standardized space (e.g. original Talairach, MNI305, ICBM152) OR indicate that the data were not normalized.*
Noise and artifact removal	*Describe your procedure(s) for artifact and structured noise removal, specifying motion parameters, tissue signals and*

Noise and artifact removal | *physiological signals (heart rate, respiration).*

Volume censoring | *Define your software and/or method and criteria for volume censoring, and state the extent of such censoring.*

Statistical modeling & inference

Model type and settings | *Specify type (mass univariate, multivariate, RSA, predictive, etc.) and describe essential details of the model at the first and second levels (e.g. fixed, random or mixed effects; drift or auto-correlation).*

Effect(s) tested | *Define precise effect in terms of the task or stimulus conditions instead of psychological concepts and indicate whether ANOVA or factorial designs were used.*

Specify type of analysis: ☐ Whole brain ☐ ROI-based ☐ Both

Statistic type for inference (See Eklund et al. 2016) | *Specify voxel-wise or cluster-wise and report all relevant parameters for cluster-wise methods.*

Correction | *Describe the type of correction and how it is obtained for multiple comparisons (e.g. FWE, FDR, permutation or Monte Carlo).*

Models & analysis

n/a	Involved in the study
☐	☐ Functional and/or effective connectivity
☐	☐ Graph analysis
☐	☐ Multivariate modeling or predictive analysis

Functional and/or effective connectivity | *Report the measures of dependence used and the model details (e.g. Pearson correlation, partial correlation, mutual information).*

Graph analysis | *Report the dependent variable and connectivity measure, specifying weighted graph or binarized graph, subject- or group-level, and the global and/or node summaries used (e.g. clustering coefficient, efficiency, etc.).*

Multivariate modeling and predictive analysis | *Specify independent variables, features extraction and dimension reduction, model, training and evaluation metrics.*